

## RESEARCH ARTICLE

# Context-specific function of the LIM homeobox 1 transcription factor in head formation of the mouse embryo

Nicolas Fossat<sup>1,2,‡,§</sup>, Chi Kin Ip<sup>1,2,‡</sup>, Vanessa J. Jones<sup>1</sup>, Joshua B. Studdert<sup>1</sup>, Poh-Lynn Khoo<sup>1</sup>, Samara L. Lewis<sup>1</sup>, Melinda Power<sup>1</sup>, Karin Tourle<sup>1</sup>, David A. F. Loebel<sup>1,2</sup>, Kin Ming Kwan<sup>3,\*</sup>, Richard R. Behringer<sup>3</sup> and Patrick P. L. Tam<sup>1,2</sup>

## ABSTRACT

*Lhx1* encodes a LIM homeobox transcription factor that is expressed in the primitive streak, mesoderm and anterior mesendoderm of the mouse embryo. Using a conditional *Lhx1* flox mutation and three different Cre deleters, we demonstrated that LHX1 is required in the anterior mesendoderm, but not in the mesoderm, for formation of the head. LHX1 enables the morphogenetic movement of cells that accompanies the formation of the anterior mesendoderm, in part through regulation of *Pcdh7* expression. LHX1 also regulates, in the anterior mesendoderm, the transcription of genes encoding negative regulators of WNT signalling, such as *Dkk1*, *Hesx1*, *Cer1* and *Gsc*. Embryos carrying mutations in *Pcdh7*, generated using CRISPR-Cas9 technology, and embryos without *Lhx1* function specifically in the anterior mesendoderm displayed head defects that partially phenocopied the truncation defects of *Lhx1*-null mutants. Therefore, disruption of *Lhx1*-dependent movement of the anterior mesendoderm cells and failure to modulate WNT signalling both resulted in the truncation of head structures. Compound mutants of *Lhx1*, *Dkk1* and *Ctnnb1* show an enhanced head truncation phenotype, pointing to a functional link between LHX1 transcriptional activity and the regulation of WNT signalling. Collectively, these results provide comprehensive insight into the context-specific function of LHX1 in head formation: LHX1 enables the formation of the anterior mesendoderm that is instrumental for mediating the inductive interaction with the anterior neuroectoderm and LHX1 also regulates the expression of factors in the signalling cascade that modulate the level of WNT activity.

**KEY WORDS:** Head formation, Anterior mesendoderm, LHX1, Transcription factor, Protocadherin, WNT signalling, CRISPR

## INTRODUCTION

WNT activity is important for regulating cell proliferation, differentiation and polarity (van Amerongen and Nusse, 2009), and for the anterior-posterior patterning of vertebrate embryos (Kiecker and Niehrs, 2001; Petersen and Reddien, 2009; Hikasa and Sokol, 2013). In the mouse, formation of the embryonic head requires stringent control of the level of WNT signalling during early postimplantation development (Fossat et al., 2011b, 2012;

Arkell et al., 2013). Elevated WNT signalling is incompatible with anterior development. In *Six3*-deficient mutants, ectopic expression of *Wnt1* is associated with the truncation of forebrain structures (Lagutin et al., 2003). In embryos lacking *Dkk1*, which encodes a secreted WNT antagonist, the region of the head rostral to the midbrain is truncated (Mukhopadhyay et al., 2001). DKK1 forms a complex with LRP6-KREMEN1, which sequesters the WNT co-receptor LRP6, preventing the formation of a functional frizzled-LRP receptor complex for signal transduction via β-catenin, thereby blocking WNT signalling (Zorn, 2001). Point mutations of *Lrp6* and *Ctnnb1* (which encodes β-catenin), which result in gain of function of the co-receptor and the transducer, respectively, are associated with head truncation (Fossat et al., 2011b). The interaction between *Dkk1*, *Lrp6* and *Ctnnb1* mutations (Fossat et al., 2011b) points to a crucial role of WNT/β-catenin signalling in head development and that elevated WNT activity underpins the failure to form the embryonic head.

Consistent with the concept that suppression of WNT signalling activity is required for head morphogenesis, the expression of several WNT inhibitors (*Dkk1*, *Cer1*, *Sfrp1* and *Sfrp5*) is regionalised to anterior germ layer tissues, whereas the expression of ligands (*Wnt3*, *Wnt3a* and *Wnt5*) is principally in posterior tissues (Mukhopadhyay et al., 2003; Kemp et al., 2005; Petersen and Reddien, 2009). Before gastrulation, cells of the extra-embryonic anterior visceral endoderm (AVE) express WNT inhibitors (Pfister et al., 2007). During gastrulation, the AVE is replaced by a mixed population of cells called the anterior mesendoderm (AME) that comprises the axial mesendoderm and the definitive endoderm. The AME, like the AVE, produces WNT inhibitors and is instrumental in inducing and maintaining the anterior characteristics of the neuroectoderm during the morphogenesis of head structures (Camus et al., 2000).

*Lhx1* (also known as *Lim1*) encodes a LIM homeobox transcription factor. Loss of *Lhx1* function results in head truncation (Shawlot and Behringer, 1995) that phenocopies loss of *Dkk1* function. Chimera studies show that normal head development requires *Lhx1* function in both the AVE and the epiblast (Shawlot et al., 1999). Cre-mediated ablation of *Lhx1* specifically in epiblast-derived tissues also produces a head truncation phenotype (Kwan and Behringer, 2002; Tanaka et al., 2010), but the developmental process underpinning the mutant phenotype has not been investigated and it is not known whether *Lhx1* is required specifically in either the mesoderm or the AME, which are both derived from the epiblast. LHX1 forms a complex with LDB1 and SSBP3 (also known as SSDP1) that regulates the expression of target genes (Hobert and Westphal, 2000; Enkhmandakh et al., 2006). Like *Lhx1*<sup>−/−</sup> embryos, *Ldb1*<sup>−/−</sup> and *Ssbp3*<sup>−/−</sup> embryos also display truncation of head structures

<sup>1</sup>Embryology Unit, Children's Medical Research Institute, Westmead, New South Wales 2145, Australia. <sup>2</sup>Discipline of Medicine, Sydney Medical School, University of Sydney, Sydney, New South Wales 2006, Australia. <sup>3</sup>Department of Genetics, MD Anderson Cancer Center, University of Texas, Houston, TX 77005, USA.

\*Present address: School of Life Sciences, The Chinese University of Hong Kong, Hong Kong SAR, China.

‡These authors contributed equally to this work

§Author for correspondence (nfossat@cmri.org.au)

Received 9 December 2014; Accepted 19 April 2015

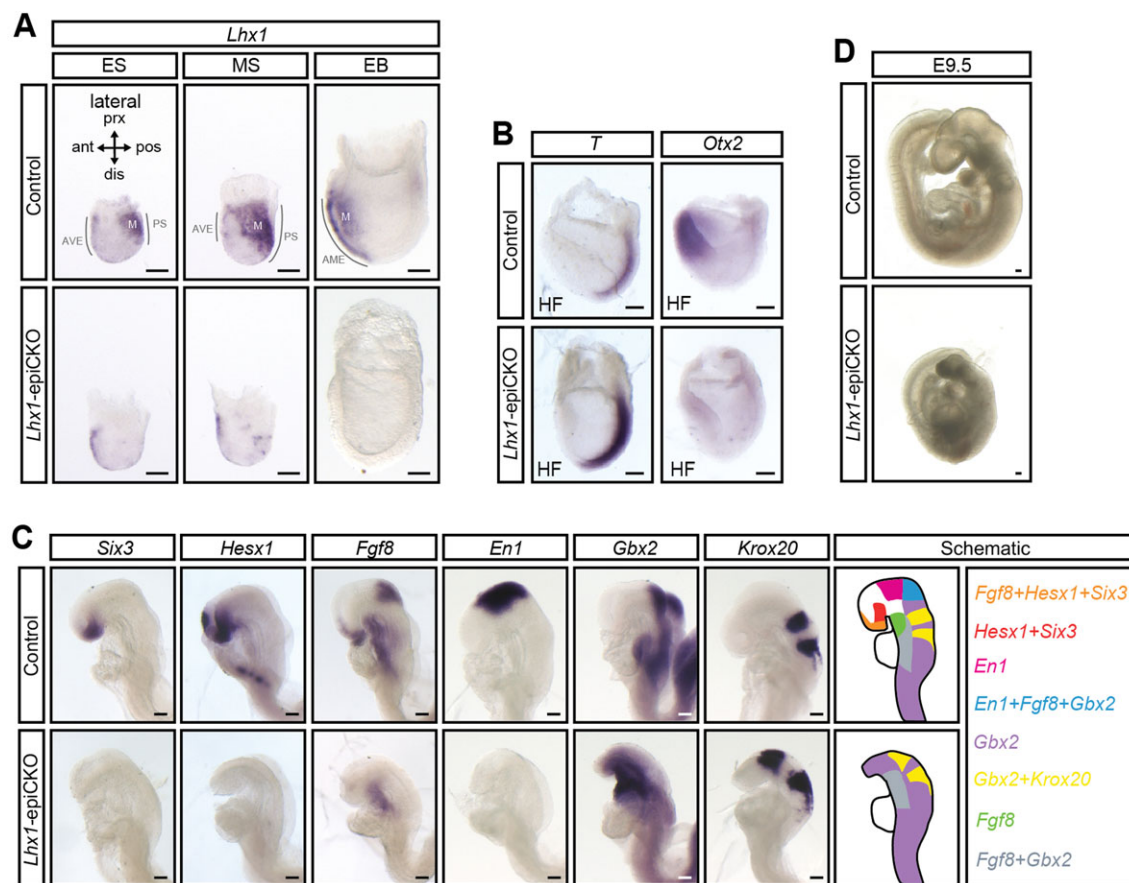


**Fig. 1. Conditional ablation of *Lhx1* activity in *Lhx1*-epiCKO mouse embryos.** (A) *Lhx1* expression in early-streak (ES), mid-streak (MS) and early-bud (EB) stage control embryos and the loss of expression in epiblast-derived tissues of *Lhx1*-epiCKO embryos. (B) Normal expression of *T* in the primitive streak and reduced expression of *Otx2* in the anterior neuroectoderm of E7.75 head-fold (HF) stage *Lhx1*-epiCKO embryos. (C) Expression of *Six3*, *Hesx1* and *Fgf8* (forebrain markers), *En1* (midbrain marker), *En1* and *Fgf8* (mid-hindbrain junction markers) and *Gbx2* and *Krox20* (hindbrain markers) in E8.5 (5- to 8-somite) control and *Lhx1*-epiCKO embryos. The schematic summarises the expression pattern of the markers (colour-coded by gene name). (D) The head truncation phenotype of E9.5 *Lhx1*-epiCKO embryos. All panels show a lateral view with anterior to the left. ant, anterior; pos, posterior; prx, proximal; dis, distal; AVE, anterior visceral endoderm; M, mesoderm; PS, primitive streak; AME, anterior mesendoderm. Scale bars: 100 μm.

(Mukhopadhyay et al., 2003; Nishioka et al., 2005). In *Ldb1* mutants, the expression of genes that encode WNT inhibitors (*Frzb*, *Sfrp1*, *Sfrp2*, *Cer1* and *Dkk1*) is reduced; and in *Ssbp3* mutants, *Dkk1* expression is lost from the prechordal plate (Mukhopadhyay et al., 2003; Nishioka et al., 2005). These findings suggest that elevated WNT signalling might be contributing to the truncation of anterior structures in embryos that have lost *Lhx1*-related function.

In the present study, we show that loss of *Lhx1* in the epiblast results in a failure to form the AME. Head formation is affected in these mutants, which may be due to the lack of expression of WNT antagonists that are normally expressed in the AME. By inactivating *Lhx1* in the AME after it is formed, we show that these mutants also display head truncation, which is accompanied by a failure to activate the expression of *Lhx1* downstream genes, including the WNT antagonists. Genetic interaction studies provide further evidence that LHX1 activity intersects with the WNT/β-catenin signalling pathway. Our findings have revealed the context-specific functions of LHX1 in the formation of the AME and in the transcriptional regulation of genes encoding WNT antagonists in the AME. In both modes of action, LHX1 engages with the modulation of WNT signalling activity, which influences the formation of the embryonic head.

## RESULTS

### Loss of *Lhx1* activity in the epiblast causes head truncation

Before gastrulation, *Lhx1* is expressed in the extra-embryonic AVE (supplementary material Fig. S1). During gastrulation, *Lhx1* expression is initially detected in the proximal-posterior epiblast where the primitive streak will form, and subsequently in the nascent mesoderm and the AME (supplementary material Fig. S1). *Lhx1* expression is not detected in the ectoderm (supplementary material Fig. S1).

To investigate the tissue-specific requirement of *Lhx1* in the epiblast and its derivatives, we studied the phenotype of embryos in which *Lhx1* activity was ablated in the epiblast by *Meox2-Cre* activity (*Lhx1*<sup>fl/fl</sup>; *Meox2*<sup>+/Cre</sup>, hereafter *Lhx1*-epiCKO embryo). In mid-streak stage mutant embryos, *Lhx1* expression was maintained in the AVE (Fig. 1A) but was drastically reduced in the mesoderm. In early-bud stage *Lhx1*-epiCKO embryos, *Lhx1* expression was completely lost from the mesoderm and the AME (Fig. 1A). At gastrulation, *Lhx1*-epiCKO embryos were similar in size and morphology to controls (Fig. 1A) and formed a primitive streak (that expressed *T*; Fig. 1B). However, little or no expression of *Otx2* was detected in the anterior ectoderm (Fig. 1B), indicating a loss of anterior neural tissue potency (Iwafuchi-Doi et al., 2012). Marker analysis of E8.5 *Lhx1*-epiCKO embryos revealed the loss

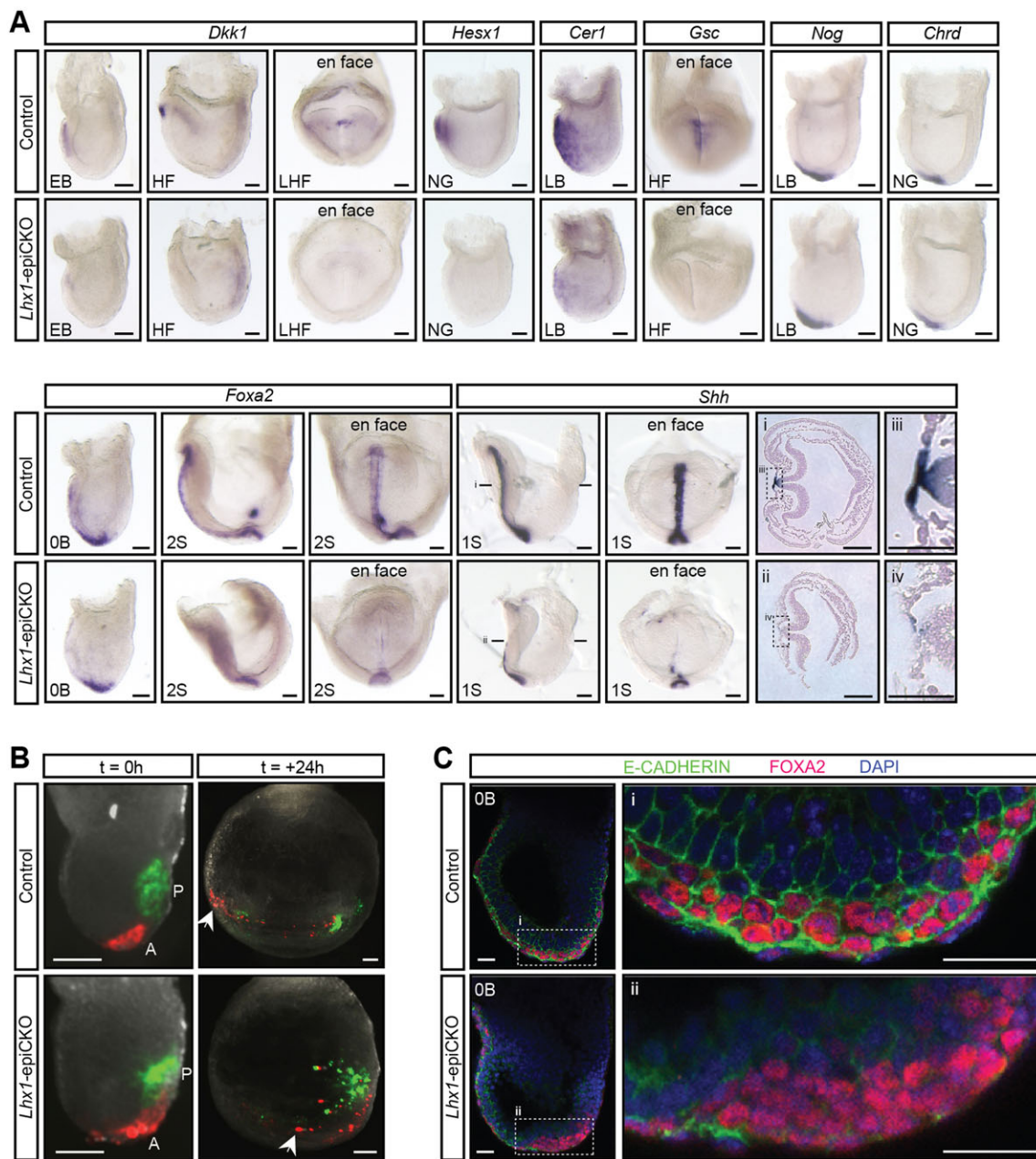


**Fig. 2. Development of anterior midline tissues in *Lhx1*-epiCKO embryos.** (A) Expression of *Dkk1*, *Hesx1*, *Cer1*, *Gsc*, *Nog*, *Chrd*, *Foxa2* and *Shh* in E7.75–E8.0 control and *Lhx1*-epiCKO embryos at the following stages: early-bud (EB), head-fold (HF); late head-fold (LHF); neural groove (NG); late-bud (LB); no-bud (0B); one-somite (1S); two-somite (2S). For *Shh* expression, the plane of the transverse sections shown in i and ii is marked on the lateral view of the whole-mount specimen. The boxed regions in i and ii are magnified in iii and iv. (B) Dye-labelled endoderm cells overlying the anterior (A, red fluorescence) and posterior (P, green fluorescence) segments of the primitive streak of mid-streak stage control and *Lhx1*-epiCKO embryos at *t*=0 h (the time the cells were labelled) and the distribution of labelled cells of the same embryos after 24 h of *in vitro* culture (*t*=+24 h). Arrowheads indicate the site of anteriormost migration of the endoderm cells originating from cells overlying the anterior segment of the primitive streak (the presumptive AME progenitor). (C) Confocal image of no-bud stage control embryo showing incorporation of the FOXA2-expressing (red in the nucleus) cells into the endoderm (E-cadherin, green on the cell membrane). By contrast, the bulk of FOXA2-expressing cells were retained in the primitive streak of *Lhx1*-epiCKO embryos. Nuclei are stained by DAPI (blue). The boxed regions are magnified in i and ii. All panels show a lateral view of whole-mount specimens and sections with anterior to the left, except for the en face views in A. Scale bars: 100 µm in A (except iii,iv) and B; 50 µm in Aiii,iv and C.

of the precursor of the dorsal and ventral forebrain (indicated by *Six3*, *Hesx1*, *Fgf8* expression), the midbrain (*En1*) and the mid-hindbrain junction (*En1*, *Fgf8*), whereas that of the hindbrain [*Gbx2*, *Krox20* (also known as *Egr2*)] was relatively intact (Fig. 1C). At E9.5, the *Lhx1*-epiCKO embryos displayed a fully penetrant head truncation phenotype (Fig. 1D; supplementary material Table S1).

#### Loss of *Lhx1* disrupts the formation of anterior midline tissues

In the anterior region of *Lhx1*-epiCKO embryos at E7.5–E7.75, before the manifestation of the abnormal head phenotype, the expression of *Dkk1*, *Hesx1*, *Cer1* and *Gsc* was lost or reduced (Fig. 2A). Although cells expressing *Nog*, *Chrd* and *Foxa2* were present in the node and in the midline tissue immediately anterior to

the node of the gastrula stage embryo, *Foxa2* and *Shh* expression was missing from the rostral tissues of the early-somite stage embryo (Fig. 2A). No *Shh*-expressing cells were present in the midline beneath the floor plate of the neural folds (Fig. 2Ai–iv). These findings suggest that *Lhx1*-deficient cells might be unable to form the AME.

To further investigate this possibility, we labelled the endoderm overlying the anterior segment of the primitive streak of the mid-streak stage embryo, where the precursors of the AME initially reside following recruitment from the epiblast (Tam et al., 2007) (Fig. 2B). After 24 h of *in vitro* culture, the labelled cells in control embryos ( $n=8$ ) were distributed along the full extent of the anterior-posterior axis, whereas their counterparts in *Lhx1*-epiCKO embryos ( $n=7$ ) failed to extend anteriorly but remained in the posterior region of the embryo (Fig. 2B). During gastrulation, the axial mesendoderm and the definitive endoderm are formed by recruiting *Foxa2*-expressing cells from the epiblast, which then transit through the primitive streak and expand after integration into the endoderm layer to populate the AME (Fig. 2C;  $n=5$ ) (Burtscher and Lickert, 2009; Viotti et al., 2014). In *Lhx1*-epiCKO mutants the endoderm contained a sparse population of FOXA2-positive cells, while the bulk of the FOXA2-positive cells remained in the primitive streak (Fig. 2C;  $n=5$ ). The absence of *Shh*- and *Foxa2*-expressing axial mesendoderm in *Lhx1*-epiCKO embryos might therefore be a consequence of the impaired morphogenetic movement of the *Lhx1*-deficient AME progenitor cells.

In *Xenopus* embryos, knockdown of *XLim1* (the *Lhx1* orthologue) leads to a headless phenotype that is accompanied by a lack of anterior extension of the chordamesoderm (the equivalent of the axial mesendoderm of the mouse). This morphogenetic defect can be rescued by expressing *XPapc*, a protocadherin in the planar cell polarity pathway, which promotes anterior extension of the *XLim1*-deficient chordamesoderm tissue (Hukriede et al., 2003). In the mouse embryo, *Pcdh8* (the orthologue of *XPapc*) is expressed only in the mesoderm (supplementary material Fig. S2C) (Hukriede et al., 2003) and, although it is downregulated in the *Lhx1*-null mutant (Hukriede et al., 2003), loss of *Pcdh8* function has no impact on head development (Yamamoto et al., 2000). We therefore examined the possibility that, in mouse, LHX1 controls the expression of other protocadherins that may be required for head formation.

*Pcdh8* belongs to the Pcdh $\delta$  family, which has nine members (Morishita and Yagi, 2007). It also has two putative paralogues, *Pcdh12* and *Pcdh20* (Fliceck et al., 2013). Expression of all of these Pcdh genes was detectable by RT-PCR in E7.75 mouse embryos (supplementary material Fig. S2A). In P19 embryonal carcinoma cells that were transfected with constructs encoding LHX1 alone or in combination with the two co-factors, LDB1 and SSBP3, only *Pcdh7*, *Pcdh8* and *Pcdh19* were activated by LHX1 or LHX1 plus its co-factors as compared with control transfections (Fig. 3A; supplementary material Fig. S2B).

We next investigated the expression of these Pcdh genes in embryos. During gastrulation, *Pcdh7* is expressed, like *Lhx1*, in the mesoderm and the AME (Fig. 3B), but *Pcdh19* and *Pcdh8* are expressed only in the mesoderm (supplementary material Fig. S2C). Focusing on *Pcdh7*, we found that its expression was reduced in *Lhx1*-epiCKO embryos (Fig. 3C). We identified two regions in the *Pcdh7* locus that are conserved between mouse and human and contain LHX1 recognition motifs (YTAATNN; where Y is C or T and NN is TA, TG, CA, GG or GA) (Mochizuki et al., 2000; Sudou et al., 2012; Yasuoka et al., 2014); they were localised  $\sim$ 0.2 kb upstream ( $-0.2R$ ) and  $\sim$ 8.5 kb downstream ( $+8.5R$ ) of the *Pcdh7* START codon (Fig. 3D; supplementary material Fig. S3).

Chromatin immunoprecipitation (ChIP)-qPCR analysis was performed with an anti-HA antibody on P19 cells that were transfected with a plasmid expressing HA-tagged wild-type (LHX1-HA) or HA-tagged mutant (LHX1 $\Delta$ -HA, lacking DNA- and protein-binding domains) LHX1 protein. Both  $-0.2R$  and  $+8.5R$  regions were bound by LHX1 but not LHX1 $\Delta$  (Fig. 3E). Furthermore, both regions could mediate the activation of a luciferase reporter by LHX1, but not LHX1 $\Delta$  (Fig. 3F).

We then tested the functional requirement for *Pcdh7* in embryonic development. Using CRISPR-Cas9 editing (Ran et al., 2013), two independent embryonic stem cell (ESC) clones, each harbouring frameshift mutations immediately downstream of the START codon on both alleles of *Pcdh7* (supplementary material Fig. S4), were generated. Chimeric embryos were produced by introducing these ESC clones into 8-cell host embryos expressing a *Rosa26-lacZ* transgene, which allowed an unequivocal assessment of the contribution of the *lacZ*-negative ESCs to the embryo proper (see Materials and Methods; Fig. 3G). E9.5 chimeras that were composed almost entirely of mutant ESCs displayed a reduced forebrain and an open neural tube (Fig. 3G; *Pcdh7* $^{+/-}$ ;  $n=3$ , *Pcdh7* $^{+/+}$ ;  $n=4$ ). This phenotype was not observed in control chimeras generated with the parental ESC line (Fig. 3G; wild type  $n=3$ ). In 7/9 E7.75 embryos generated with the mutant ESCs, a shorter *Shh*-positive midline structure was formed than in stage-matched control embryos ( $n=5$ ) (Fig. 3H). Altogether, these results suggest that the reduction of *Pcdh7* expression in *Lhx1*-epiCKO embryos might contribute to the defect in AME formation and the head truncation phenotype.

#### ***Lhx1* function is required in the AME for head formation**

In gastrula stage embryos, *Lhx1* is expressed in the mesoderm and the AME (supplementary material Fig. S1). To study the requirement for *Lhx1* in these two tissues, we generated mutant embryos in which *Lhx1* was ablated either in the mesoderm or the AME. To inactivate *Lhx1* flox in the mesoderm, we used a *Cre* recombinase that is expressed from the *Mesp1* locus (Saga et al., 1999). Mesoderm cells that express *Mesp1-Cre* have been shown to contribute extensively to the cranial mesenchyme (Saga et al., 1999; Bildsoe et al., 2013). In the mesoderm conditional mutant (*Lhx1* $^{flox/-}$ ; *Mesp1* $^{+/-}$ , hereafter *Lhx1*-mesCKO) embryos, *Lhx1* expression was detected initially in the nascent mesoderm adjacent to the primitive streak (supplementary material Fig. S5A, LS) but was lost in the fully formed mesoderm, whereas expression was retained in the AME (supplementary material Fig. S5A, OB, EB-LB). Despite the loss of *Lhx1* expression in the mesoderm, *Lhx1*-mesCKO embryos were morphologically indistinguishable from controls (supplementary material Fig. S5B), suggesting that *Lhx1* function in the mesoderm is unlikely to be crucial for head development.

To assess the function of *Lhx1* in the AME, the *Lhx1* flox allele was ablated by tamoxifen-activated MerCreMer (mcm) recombinase expressed from the *Foxa2* locus (Park et al., 2008). *Foxa2* is expressed in the AME and the endoderm, but not the mesoderm (Burtscher and Lickert, 2009). Expression of the *lacZ* reporter in tamoxifen-treated *Foxa2* $^{+/-}$ ; *Rosa26* $^{+/-}$  embryos showed that MerCreMer was activated widely in the endoderm layer of the embryo, which encompassed the *Lhx1*-expressing AME tissues (Fig. 4A) (Park et al., 2008; Ip et al., 2014). When *Lhx1* $^{flox/flox}$  mice were crossed with *Lhx1* $^{+/-}$ ; *Foxa2* $^{+/-}$  mice or *Lhx1* $^{+/-}$ ; *Foxa2* $^{mcm/mcm}$  mice, embryos of four genotypes (*Lhx1* $^{+/-}$ ; *Foxa2* $^{+/-}$ , *Lhx1* $^{flox/-}$ ; *Foxa2* $^{+/-}$ , *Lhx1* $^{+/-}$ ; *Foxa2* $^{+/-}$ , *Lhx1* $^{flox/-}$ ; *Foxa2* $^{+/-}$ ) were obtained. Twenty-eight hours after injection at E6.5, *Lhx1* expression was markedly reduced or absent in the AME

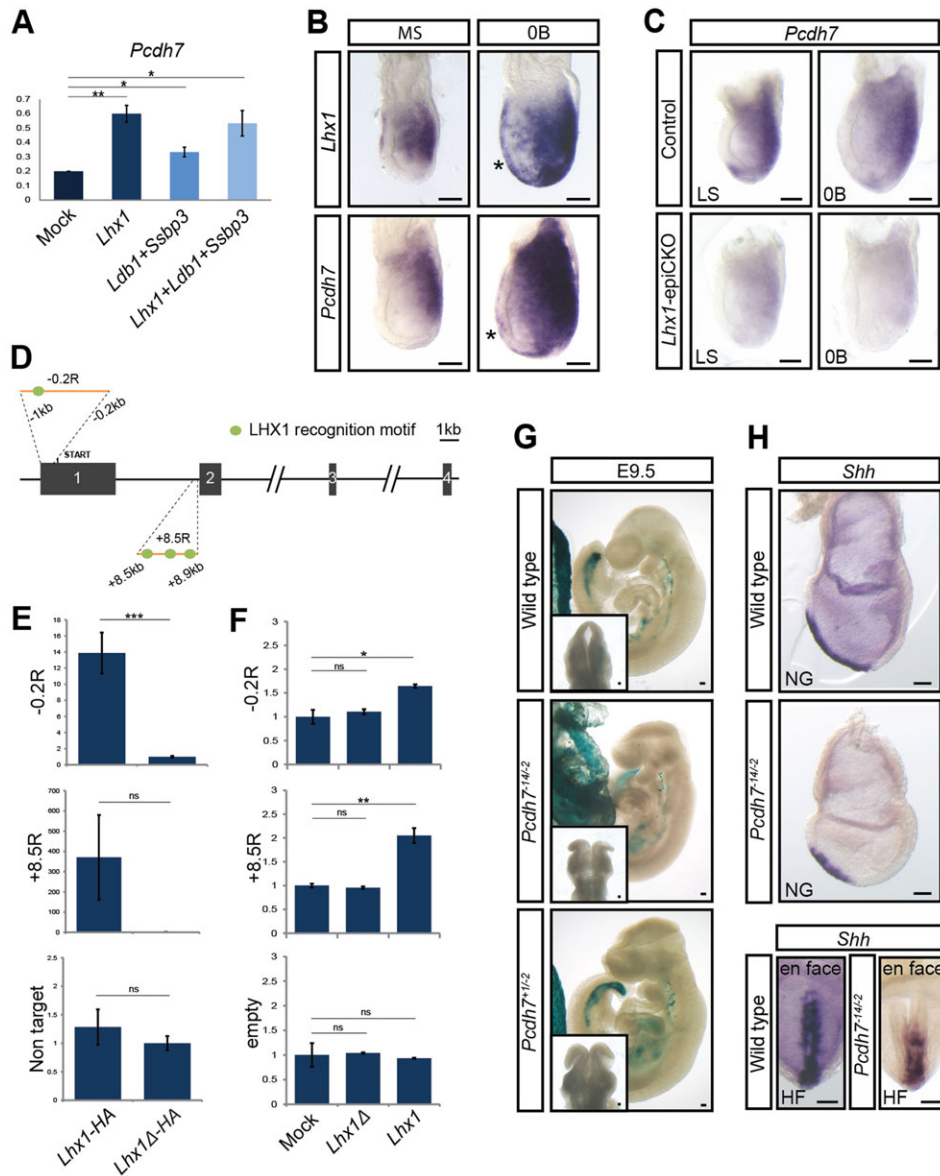


**Fig. 3. *Pcdh7* and head formation.** (A) Expression of *Pcdh7* (relative to β-actin) analysed by RT-qPCR in P19 cells transfected with different combinations of vectors expressing a mock protein, *Lhx1*, *Ldb1+Ssbp3* and *Lhx1+Ldb1+Ssbp3*. (B) *Lhx1* and *Pcdh7* show overlapping expression in the mesoderm and the AME (asterisk) in mid-streak (MS) and no-bud (0B) stage embryos. (C) *Pcdh7* expression was reduced in *Lhx1-epiCKO* embryos. LS, late-streak stage. (D) Genomic structure of the mouse *Pcdh7* locus. Coordinates are indicated relative to the START codon. Grey boxes, exons; orange lines, the conserved regions analysed in E and F; green circles, LHX1 recognition motifs. (E) qPCR of *Pcdh7* regions -0.2R and +8.5R and a region not bound by LHX1 (non target) following immunoprecipitation with an anti-HA antibody from P19 cells that were co-transfected with *Ldb1+Ssbp3+Lhx1-HA* or *Ldb1+Ssbp3+Lhx1Δ-HA* expression vectors. Results are normalised to qPCR results of input samples. (F) Firefly luciferase activity (relative to *Renilla* luciferase) in P19 cells co-transfected with pGL3 vector (empty) or containing the *Pcdh7* -0.2R or the *Pcdh7* +8.5R region, a *Renilla* expression vector and different combinations of vectors expressing a mock protein, *Lhx1Δ* or *Lhx1*. (G) ESCs (*lacZ*-negative)→*Rosa26* (*lacZ*-positive) chimeras at E9.5. Chimeras with a predominant contribution of *lacZ*-negative mutant cells (*Pcdh7*<sup>-14/-2</sup> or *Pcdh7*<sup>+/12</sup>) to the embryo proper showed reduced head size, an open neural tube (dorsal view of the head region in insets) and were missing forebrain structure. Chimeras with a predominant contribution of *lacZ*-negative wild-type cells developed a normal head. (H) E7.75 chimeras generated with *Pcdh7* mutant cells have a shorter *Shh*-expressing midline structure than chimeras generated with wild-type ESCs. Bottom panels are *en face* views of the embryo. NG, neural-groove stage; HF, head-fold stage. (A,E,F) Data are presented as the mean±s.e. of n=3 independent experiments for each condition of transfection. \*P<0.05, \*\*P<0.01, \*\*\*P<0.001, no significant difference (ns) by t-test. All panels show a lateral view with anterior to the left, except for the insets in G and the *en face* views in H. Scale bars: 100 μm.

of tamoxifen-treated *Lhx1*<sup>flx/-</sup>; *Foxa2*<sup>+/mcm</sup> (*Lhx1*-ameCKO) embryos, as compared with mock-treated (vehicle only) *Lhx1*<sup>flx/-</sup>; *Foxa2*<sup>+/mcm</sup> or tamoxifen-treated *Lhx1*<sup>flx/-</sup>; *Foxa2*<sup>+/+</sup> controls (Fig. 4B). At E9.5, 90% of the *Lhx1*-ameCKO embryos displayed some degree of head truncation (Fig. 4C,D; supplementary material Table S2). The expression of forebrain markers was lost or reduced in the *Lhx1*-ameCKO embryos

(Fig. 4E). These results highlight an essential role for *Lhx1* in the AME for head formation.

We next examined the AME of the *Lhx1*-ameCKO embryos. In contrast to *Lhx1*-epiCKO embryos, the *Lhx1*-ameCKO embryos formed an *Shh*-expressing midline structure similar to the anterior midline of control embryos (Fig. 4F). However, *in situ* hybridisation showed that the expression of *Dkk1*, *Hesx1*, *Cer1* and *Gsc* was

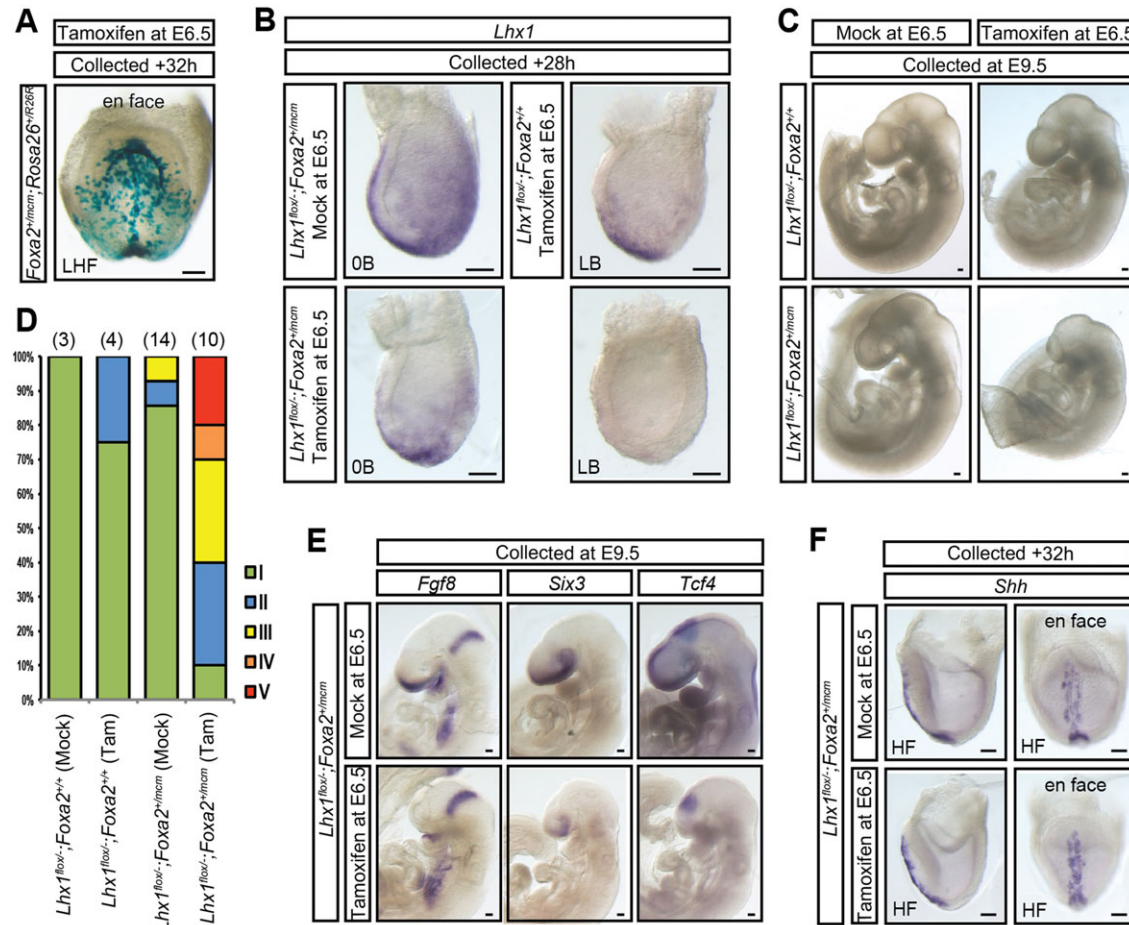


**Fig. 4. Conditional ablation of *Lhx1* in the AME.** (A) X-Gal-positive cells in the AME of *Foxa2*<sup>+/-</sup>; *Rosa26*<sup>+/R26R</sup> embryos 32±2 h after tamoxifen treatment at E6.5. LHF, late head-fold stage. (B) Expression of *Lhx1* in *Lhx1*<sup>fl/fl</sup>; *Foxa2*<sup>+/+</sup> and *Lhx1*<sup>fl/fl</sup>; *Foxa2*<sup>+/-</sup> embryos 28±2 h after injection of tamoxifen or vehicle only (mock) at E6.5. 0B, no-bud stage; LB, late-bud stage. (C) Head morphology of E9.5 *Lhx1*<sup>fl/fl</sup>; *Foxa2*<sup>+/+</sup> and *Lhx1*<sup>fl/fl</sup>; *Foxa2*<sup>+/-</sup> embryos after tamoxifen or mock injection at E6.5. Severe head truncation (bottom right panel) was observed only in tamoxifen-treated *Lhx1*<sup>fl/fl</sup>; *Foxa2*<sup>+/-</sup> (*Lhx1*-ameCKO) embryos. (D) The distribution of embryos of the different genotypes (x-axis) to the five head phenotype categories based on the size of the forebrain and midbrain: I, normal size; II, slight reduction (<25%); III, strong reduction (26–75% reduction); IV, tissue remnant (>75% reduction); V, tissues absent. The number of embryos scored for each genotype is given in parentheses. (E) Expression of *Fgf8* and *Six3* (telencephalon markers), *Tcf4* (diencephalon marker) and *Fgf8* (mid-hindbrain junction marker) in E9.5 mock and tamoxifen-treated *Lhx1*<sup>fl/fl</sup>; *Foxa2*<sup>+/-</sup> embryos. (F) Presence of *Shh*-expressing tissues in the anterior midline of *Lhx1*<sup>fl/fl</sup>; *Foxa2*<sup>+/-</sup> embryos 32±2 h after mock or tamoxifen treatment at E6.5. HF, head-fold stage. All panels show a lateral view with anterior to the left, except for the en face views in A and F. Scale bars: 100 µm.

reduced in the mutant embryos (Fig. 5A), which was confirmed by RT-qPCR analysis (Fig. 5B). Furthermore, we showed that *Lhx1* expression, in combination with *Ldb1* and *Ssbp3*, could activate these four genes in P19 cells (Fig. 5C).

*Hesx1* is a known LHX1 target in mouse. LHX1 binds the dTAAT and pTAAT elements (referred to hereafter as the dp region) of the *Hesx1* locus (Fig. 5D) (Chou et al., 2006). As expected, ChIP-PCR in P19 cells using the anti-HA antibody and the LHX1-HA expression constructs confirmed the binding of LHX1 to the dp region of the *Hesx1* locus (Fig. 5E). *Cer1* and *Gsc* have also been reported to be directly regulated by XLIM1 in *Xenopus*, which binds to a region referred to as U1 (Sudou et al., 2012). The U1 region of *Gsc* is conserved in mouse and is also recognised by LHX1 (Fig. 5D,E; supplementary material Fig. S6A). However, no equivalent of the U1 region of *Xenopus Cer1* (Sudou et al., 2012) was found in mouse. Instead, we showed that LHX1 could bind to a conserved region of the *Cer1* locus containing LHX1 recognition motifs located ~4 kb (+4R) after the START codon (Fig. 5D,E; supplementary material Fig. S6B).

Whether *Dkk1* is a direct downstream target of LHX1 has not previously been investigated. A conserved region of the mouse *Dkk1* locus, referred to as H1, has been shown to be necessary for the control of *Dkk1* expression (Kimura-Yoshida et al., 2005). This region is bound by another homeobox transcription factor, OTX2 (Kimura-Yoshida et al., 2005; Ip et al., 2014), which can directly interact with LHX1 to activate target genes involved in head formation (Nakano et al., 2000; Yasuoka et al., 2014). We analysed the H1 region of *Dkk1* and found two putative LHX1 recognition motifs, one localised at the distal (dH1) end and one at the proximal end (Fig. 5D; supplementary material Fig. S6C). Our results showed that LHX1 binds to dH1 but not to the proximal region in H1 (Fig. 5E; data not shown). LHX1Δ did not bind to any of the target sequences in the four genes tested (Fig. 5E). We further analysed the interaction of LHX1 with *Dkk1* and showed that the dH1 region can mediate the activation of luciferase reporter by LHX1 or LHX1+LDB1+SSBP3 but not LHX1Δ (Fig. 5F). Furthermore, a point mutation in the LHX1 recognition motif in dH1 abolished its trans-activating function (Fig. 5G).

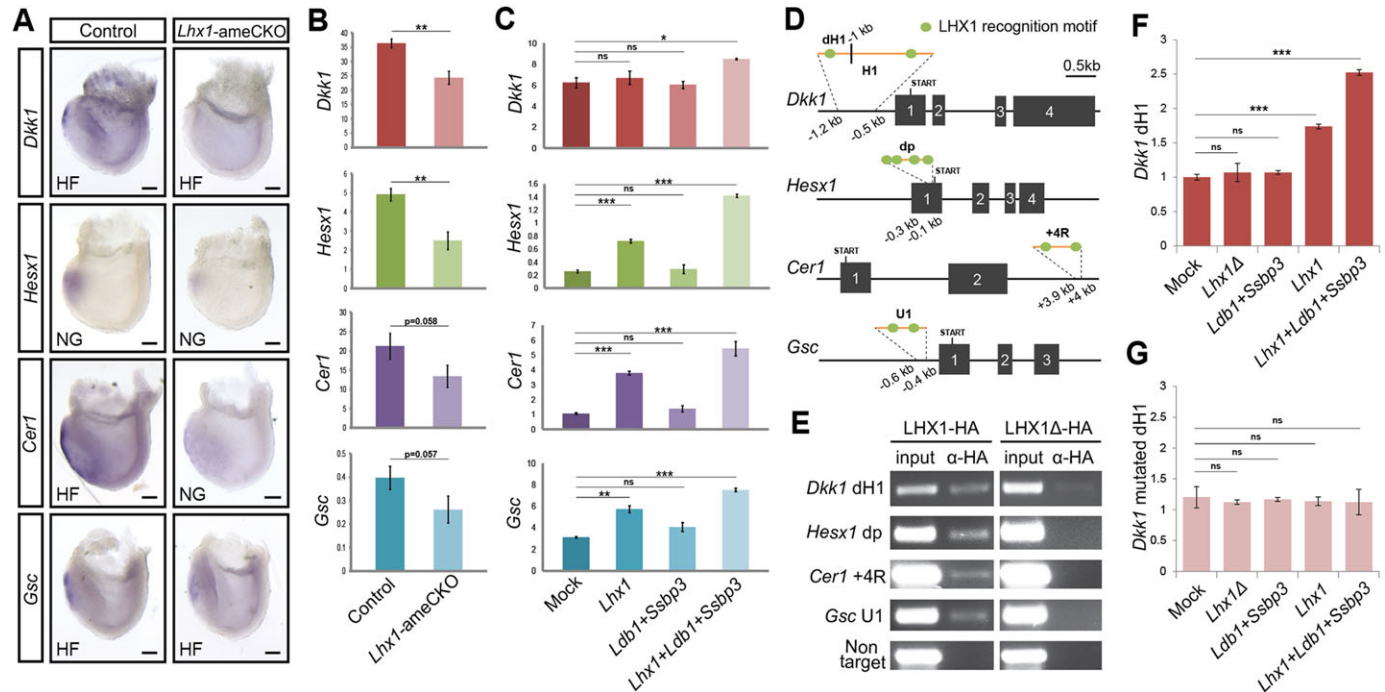


**Fig. 5. The expression of genes associated with the AME is modulated by LHX1.** (A) *In situ* hybridisation of *Dkk1*, *Hesx1*, *Cer1* and *Gsc* in neural-groove (NG) to head-fold (HF) stage control (*Lhx1*<sup>flox1</sup>–; *Foxa2*<sup>+/mcm</sup>) mock treated or (*Lhx1*<sup>flox1</sup>–; *Foxa2*<sup>+/mcm</sup>) tamoxifen treated and *Lhx1*-ameCKO (*Lhx1*<sup>flox1</sup>–; *Foxa2*<sup>+/mcm</sup>) tamoxifen treated embryos collected 32±2 h after mock or tamoxifen treatment at E6.5. Lateral views with anterior to the left. Scale bars: 100 µm. (B) RT-qPCR analysis of the expression of *Dkk1*, *Hesx1*, *Cer1* and *Gsc* (relative to β-actin) in the anterior germ layer tissues of neural-groove to head-fold stage control (*Lhx1*<sup>flox1</sup>–; *Foxa2*<sup>+/+</sup> or *Lhx1*<sup>flox1</sup>–; *Foxa2*<sup>+/mcm</sup>) and *Lhx1*-ameCKO (*Lhx1*<sup>flox1</sup>–; *Foxa2*<sup>+/mcm</sup>) embryos collected 32±2 h after tamoxifen treatment at E6.5. (C) RT-qPCR analysis of the expression of *Dkk1*, *Hesx1*, *Cer1* and *Gsc* (relative to β-actin) in P19 cells transfected with different combinations of vectors expressing a mock protein, *Lhx1*, *Ldb1+Ssdp3* and *Lhx1+Ldb1+Ssdp3*. (D) Genomic structure of the mouse *Dkk1*, *Hesx1*, *Cer1* and *Gsc* loci. Coordinates are indicated relative to the START codon. Grey boxes, exons; orange lines, the conserved regions analysed in E-G; green circles, LHX1 recognition motifs; dH1 and H1, *Dkk1* distal H1 region and H1 region; dp, *Hesx1* dTAAT and pTAAT containing region; +4R, conserved region of *Cer1*; U1, conserved region of *Gsc*. (E) ChIP-PCR analysis of the conserved regions shown in D following transfection of P19 cells with plasmids expressing *Ldb1+Ssdp3+Lhx1-HA* or *Ldb1+Ssdp3+Lhx1Δ-HA*, and PCR detection of the target sequence in input and anti-HA (α-HA) immunoprecipitated chromat. (F,G) Firefly luciferase activity (relative to *Renilla* luciferase) in P19 cells transfected with pGL3-promoter plasmid containing the *Dkk1* dH1 region (F) or the *Dkk1* dH1 region with mutated LHX1 recognition motif (G), a *Renilla* luciferase expression vector and different combinations of vectors expressing a mock protein, *Lhx1Δ*, *Lhx1*, *Ldb1* and/or *Ssdp3*. Data represent the mean±s.e. of n=5 independent embryos of each genotype (B) or n=3 independent experiments for each condition of transfection (C,F,G). \*P<0.05, \*\*P<0.01, \*\*\*P<0.001, no significant difference (ns) by t-test.

Altogether, these results suggest that LHX1 is required in the AME for head formation, where it may directly regulate the transcription of *Dkk1*, *Hesx1*, *Cer1* and *Gsc*.

#### Elevated WNT signalling activity contributes to the head phenotype in *Lhx1* mutants

*Lhx1*-epiCKO and *Lhx1*-ameCKO embryos displayed head defects similar to those of embryos affected by an excess of WNT/β-catenin signalling activity (Figs 1 and 4) (Mukhopadhyay et al., 2001; Lewis et al., 2008; Fossat et al., 2011b). In both conditional mutants, loss of *Lhx1* results in the reduced expression of genes encoding WNT antagonists (Figs 2 and 5). This finding points to a potential gain of WNT activity in the *Lhx1* mutants. Using the BATGal *lacZ* transgene, which is a reporter of WNT activity (Maretto et al., 2003), and by measuring the expression of two direct WNT targets (*Axin2* and *Lef1*) by RT-qPCR, we showed that both the reporter and the target genes are significantly upregulated in the anterior tissues of the *Lhx1*-epiCKO embryo (Fig. 6A,B). A similar, albeit not statistically significant, trend was observed for the target genes in *Lhx1*-ameCKO embryos (Fig. 6C). This is likely to be related to the incomplete penetrance of the abnormal head phenotype in these mutants (Fig. 4D; supplementary material Table S2), a conjecture that is compatible with our previous finding that the degree of head

truncation is correlated with the extent of elevation of WNT activity (Fossat et al., 2011b).

To test whether enhanced WNT signalling underlies the *Lhx1* mutant phenotype, we examined the phenotypic effect of an increase of WNT signalling in conjunction with reduced *Lhx1* activity in compound mutant embryos. *Ctnnb1* encodes β-catenin, which is the key transcriptional mediator for the activity of the WNT/β-catenin signalling cascade (Petersen and Reddien, 2009). The *Ctnnb1* *batface* (*Bfc*) gain-of-function allele is associated with an excess of WNT/β-catenin signalling activity and the homozygous *Bfc* mutant embryo displays a headless phenotype (Fossat et al., 2011b). To determine whether the effect of *Lhx1* loss is enhanced by an increase of WNT/β-catenin signalling activity, we examined the phenotype of embryos heterozygous for the *Lhx1*-null allele and the *Ctnnb1* *Bfc* allele. We found that 71% of *Lhx1*<sup>+/−</sup>; *Ctnnb1*<sup>Bfc/+</sup> compound mutant embryos displayed various degrees of head defect, whereas only 19% of *Lhx1*<sup>+/−</sup> embryos and 24% of *Ctnnb1*<sup>Bfc/+</sup> embryos were affected (Fig. 6D; supplementary material Fig. S7A and Table S3).

We also tested whether the increase in WNT signalling due to the inactivation of one allele of *Dkk1* (Mukhopadhyay et al., 2001) could also enhance the head truncation phenotype of *Lhx1* mutant embryos. We found that 74% of *Dkk1*<sup>+/−</sup>; *Lhx1*<sup>+/−</sup> compound

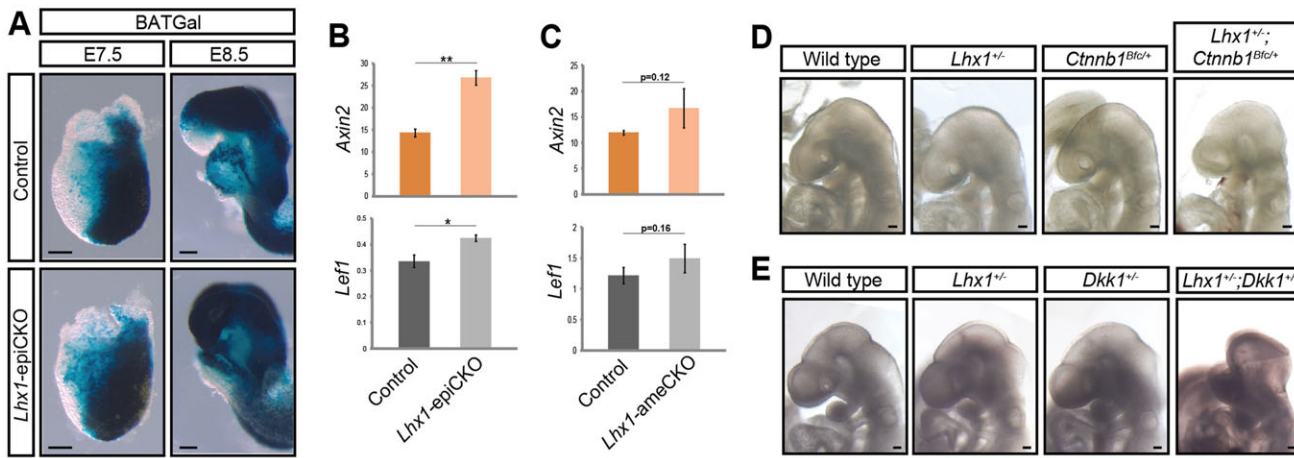


**Fig. 6. Interaction of *Lhx1* activity and WNT signalling.** (A) Expression of BATGal *lacZ* reporter in E7.5 and E8.5 *Lhx1*-epiCKO embryos. (B,C) RT-qPCR expression analysis of the WNT targets *Axin2* and *Lef1* (relative to  $\beta$ -actin) in the anterior germ layer tissues of E7.75 early-bud to head-fold stage (B) control (*Lhx1*<sup>+/-</sup>;Meox2<sup>+/-Cre</sup>) and *Lhx1*-epiCKO (*Lhx1*<sup>fl/fl</sup>;Meox2<sup>+/-Cre</sup>) embryos and (C) control (*Lhx1*<sup>fl/fl</sup>;Foxa2<sup>+/-</sup> or *Lhx1*<sup>fl/fl</sup>;Foxa2<sup>+/-mcm</sup>) and *Lhx1*-ameCKO (*Lhx1*<sup>fl/fl</sup>;Foxa2<sup>+/-mcm</sup>) embryos collected 32±2 h after tamoxifen treatment at E6.5. Data represent the mean±s.e. of n=3 independent pools of five embryos each (B) or n=5 individual embryos (C) analysed for each genotype. \*P<0.05, \*\*P<0.01, by t-test. (D) Head morphology of E9.5 wild-type, *Lhx1*<sup>+/-</sup>, *Ctnnb1*<sup>Bfcl+</sup> and compound heterozygous *Lhx1*<sup>+/-</sup>;*Ctnnb1*<sup>Bfcl+</sup> embryos. (E) Head morphology of E9.5 wild-type, *Lhx1*<sup>+/-</sup>, *Dkk1*<sup>+/-</sup> and compound heterozygous *Lhx1*<sup>+/-</sup>;*Dkk1*<sup>+/-</sup> embryos. All panels show a lateral view with anterior to the left. Scale bars: 100  $\mu$ m.

heterozygous embryos displayed abnormal head morphology, compared with 9% of *Lhx1*<sup>+/-</sup> embryos and 0% of *Dkk1*<sup>+/-</sup> embryos (Fig. 6E; supplementary material Fig. S7B,C and Table S4). At E7.75, *Axin2* expression was significantly elevated in the anterior region of the *Dkk1*<sup>+/-</sup>;*Lhx1*<sup>+/-</sup> embryos as compared with wild type (supplementary material Fig. S7D). We also generated compound *Lhx1*<sup>fl/fl</sup>;*Dkk1*<sup>+/-</sup>;Meox2<sup>+/-Cre</sup> embryos by crossing *Lhx1*<sup>fl/fl</sup> mice and *Dkk1*<sup>+/-</sup>;Meox2<sup>+/-Cre</sup> mice. In these mutants, the flox allele of *Lhx1* is ablated only in the epiblast-derived tissues that are also heterozygous for the *Dkk1*-null allele. They displayed a higher frequency of head truncation compared with the single-heterozygous embryos (supplementary material Fig. S7E,F and Table S5). The enhancement of the head phenotype might therefore be due to the additive effects of elevated WNT signalling caused by reduced *Lhx1* activity and exacerbated by a further increase in signalling activity in *Dkk1*<sup>+/-</sup> epiblast derivatives. Taken together, these results support the proposition that an increase in WNT signalling activity underpins the head truncation phenotype of *Lhx1* loss-of-function embryos.

## DISCUSSION

Our study has provided several novel insights into the role of LHX1 in head morphogenesis. We have demonstrated that LHX1 acts upstream in the WNT pathway by regulating genes encoding factors that negatively modulate the level of signalling activity. We have also shown that LHX1 is required for the formation of the anterior midline tissues in which these WNT-modulating factors are expressed. Therefore, the loss of *Lhx1* function leads to a reduction in WNT antagonistic activity, possibly via a direct effect on the transcriptional regulation of the target genes and an indirect effect resulting from the loss of tissues expressing the downstream genes (Fig. 7).

The tissue requirement of *Lhx1* for head formation during gastrulation has been studied in mouse chimeras (Shawlot et al., 1999). In that study, chimeras with an *Lhx1*<sup>-/-</sup> visceral endoderm and a wild-type epiblast displayed head defects similar to *Lhx1*<sup>-/-</sup> embryos, which is consistent with an essential requirement of *Lhx1* in the visceral endoderm for head formation (Shimono and Behringer, 2003). Complementary chimeras with wild-type

visceral endoderm and *Lhx1*<sup>-/-</sup> epiblast (*Lhx1*<sup>-/-</sup>↔+/+ chimeras) have head defects resembling those of *Lhx1*-epiCKO embryos (Shawlot et al., 1999; Kwan and Behringer, 2002; the present study). However, the formation of the AME was not specifically addressed in the *Lhx1*<sup>-/-</sup>↔+/+ chimeras (Shawlot et al., 1999). Our study on the formation of the AME was prompted by the observations that *XLIM1* is necessary for the formation of the equivalent structure in *Xenopus* and that *Lhx1*<sup>-/-</sup> anterior primitive streak tissue displays impaired tissue extension activity when transplanted into a wild-type host (Hukriede et al., 2003). We have shown that no midline structure resembling the AME is present in *Lhx1*-epiCKO embryos. Although *Foxa2*-, *Nog*- and *Chrd*-expressing progenitors of the AME are specified despite the loss of *Lhx1* from their precursors in the epiblast, these progenitor cells do not participate effectively in the morphogenetic movements that accompany the formation of the AME. The loss of *Lhx1* function might have affected the morphogenetic capacity of the *Foxa2*-expressing AME progenitors. This phenotype could be partly explained by the downregulation of *Pcdh7*, a potential LHX1 transcriptional target. *Pcdh7* is co-expressed with *Lhx1*, its expression is reduced in *Lhx1*-epiCKO mutants and *Pcdh7*-deficient embryos display head and AME defects. This demonstrates a novel requirement for *Lhx1* in the formation of the AME that might be mediated by PCDH7 (Fig. 7). In *Xenopus*, the orthologue of *Pcdh7* has been shown to play a role in cell adhesion and ectodermal cell sorting (Bradley et al., 1998; Rashid et al., 2006). Human *PCDH7* is involved in the regulation of cell shape and cell adhesion (Yoshida, 2003) and inactivation of *PCDH7* inhibits breast cancer cell migration and invasion (Li et al., 2013). Furthermore, *Xenopus* embryos in which *Pcdh7* expression is disrupted display defective neural tube closure (Rashid et al., 2006), a phenotype also observed in *Pcdh7* mutant mouse embryos.

Previous attempts to study the role of *Lhx1* in the AME have analysed the anterior tissue of *Lhx1*<sup>-/-</sup> embryos (Shawlot et al., 1999; Shimono and Behringer, 1999). However, the findings of our present study show that the AME is absent in the anterior tissue of the embryo when *Lhx1* is inactivated in the epiblast (which contains the progenitors of the AME), suggesting that the AME was not part of

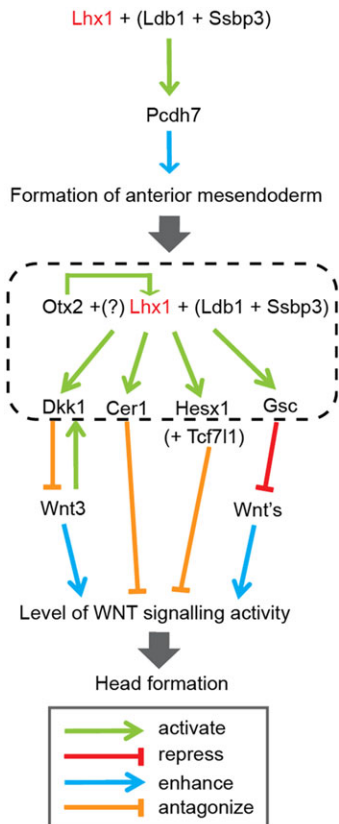


**Fig. 7. The input of LHX1 function to WNT signalling in head formation.** LHX1, in conjunction with co-factors LDB1 and SSBP3, and potentially OTX2, activates genes in the AME, which encode secreted molecules (*Dkk1*, *Cer1*) and transcription factors (*Gsc*, *Hesx1*) that negatively modulate (antagonise) the level of WNT signalling activity for head formation. *Gsc* has been demonstrated to directly repress the expression of *XWnt8*. OTX2 has been shown to directly regulate the transcription of *Lhx1*. LHX1 also regulates the expression of *Pcdh7*, a protocadherin that may be involved in the morphogenetic activity of FOXA2-expressing cells during the formation of the AME. The functional relationship of *Pcdh7* with WNT signalling is presently unknown.

the tissue fragment analysed previously. In the present work, the AME does form in *Lhx1*-ameCKO embryos and the loss of *Lhx1* in this tissue results in the development of an abnormal head. This demonstrates, for the first time, a requirement for *Lhx1* in the AME. Loss of *Lhx1* in the AME results in the downregulation of genes that encode WNT signalling antagonists, such as *Dkk1*, *Hesx1*, *Cer1* and *Gsc*. *Hesx1* is a direct target of LHX1 (Chou et al., 2006) and *Hesx1*<sup>−/−</sup> embryos display a truncated head that is associated with an increase in WNT signalling (Martinez-Barbera et al., 2000; Andoniadou et al., 2007, 2011). The *Hesx1* mutant phenotype is rescued by β-catenin inactivation and exacerbated by the deletion of *Tcf7l1* (also known as *Tcf3*), a negative regulator of WNT activity (Andoniadou et al., 2011). In *Xenopus*, *Cer1* and *Gsc* are bound and activated by XLM1 (Sudou et al., 2012). *Xenopus Cer1* encodes a secreted factor that antagonises WNT signalling (Piccolo et al., 1999). In mouse, *Cer1* activity maintains the neural characteristics of the anterior ectoderm (Shawlot et al., 2000). We have previously demonstrated that *Gsc* activity is required for patterning the forebrain (Camus et al., 2000). A reduction of both *Dkk1* and *Gsc* in the mouse embryo results in head truncation (Lewis et al., 2007), presumably owing to increased WNT signalling activity in the compound mutant with reduced activity of the antagonist and repressor of WNT ligand expression (Yao and Kessler,

2001). Results of RT-qPCR and ChIP-PCR show that LHX1 can bind to a newly identified regulatory region in *Cer1*, and *Dkk1* is likely to be a novel transcriptional target of LHX1 that acts in concert with LDB1 and SSBP3 (Mukhopadhyay et al., 2003; Nishioka et al., 2005; Enkhmandakh et al., 2006). *Dkk1*<sup>−/−</sup> embryos fail to develop a head due to an excess of WNT3 signalling (Lewis et al., 2008) and *Dkk1* and *Lhx1* mutations interact synergistically to enhance head truncation. Loss of WNT antagonists, and *Dkk1* in particular, is therefore a causative factor of head truncation in *Lhx1* mutants (Fig. 7).

Our study has shown that LHX1 enables the morphogenetic cell movements that are instrumental in the formation of the AME, which is the source of factors that fine-tune the level of WNT signalling activity (Arkell and Tam, 2012; Fossat et al., 2012; Arkell et al., 2013). In the AME, LHX1 function intersects with the WNT pathway via transcriptional control of modulators of WNT signalling activity. LHX1 binds to a regulatory region of *Dkk1* that also interacts with another transcription factor, OTX2 (Kimura-Yoshida et al., 2005; Ip et al., 2014), and OTX2 and LHX1 are part of the same activator complex (Nakano et al., 2000; Yasuoka et al., 2014). OTX2 can directly regulate *Cer1* and *Gsc* in *Xenopus* (Sudou et al., 2012; Yasuoka et al., 2014) and *Hesx1* in chicken (Spieler et al., 2004). *Lhx1* is also a target of OTX2 and its expression in the AME is regulated by OTX2 (Ip et al., 2014). Together, our findings reveal an upstream function of LHX1, which may act in conjunction with OTX2, in regulating the expression of genes that encode secreted molecules (e.g. *Dkk1*, *Cer1*) and transcription factors (e.g. *Gsc*, *Hesx1*) that are involved in the modulation of WNT/β-catenin signalling (Fig. 7).

## MATERIALS AND METHODS

### Mouse strains, genotyping and crosses

*Lhx1*<sup>fl/fl</sup> and *Lhx1*<sup>+/−</sup> (Kwan and Behringer, 2002), *Meox2*<sup>+/Cre</sup> (Tallquist and Soriano, 2000), *Mesp1*<sup>+/Cre</sup> (Saga et al., 1999), *Foxa2*<sup>+/mcm</sup> (Park et al., 2008), *Rosa26*<sup>+/R26R</sup> (Soriano, 1999), CMV-Cre (Schwenk et al., 1995), BATGal (Maretti et al., 2003), *Ctnnb1*<sup>Bf/+</sup> (Fossat et al., 2011b) and *Dkk1*<sup>+/−</sup> (Mukhopadhyay et al., 2001) mice were used. Genotyping by PCR followed established protocols and was performed on DNA extracted from tail tissues of newborn or the yolk sac of embryos. Breeding strategies for the production of mutants are outlined in supplementary material Tables S1–S5. Animal experimentation was approved by the Animal Ethics Committee of the Children's Medical Research Institute and the Children's Hospital at Westmead.

### Generation of *Pcdh7* mutant chimeric embryos using the CRISPR-Cas9 technology

Oligonucleotides 5'-CACGCCAAGCAGCTGCTCCGGTAC and 5'-AAA-CGTACCGGAGCAGCTGCTTGGC were cloned into the pSpCas9(BB)-2A-GFP (PX458) plasmid [Addgene plasmid #48138 (Ran et al., 2013)], a gift from Feng Zhang, to express the sgRNA targeted to ~100 bp downstream of the START codon of *Pcdh7* (supplementary material Fig. S3A). PX458 also expresses Cas9 and GFP. The plasmid was nucleofected into R1-129 ESCs. GFP-positive clones were isolated and analysed for mutation of the *Pcdh7* locus. Two clones with biallelic frameshift mutations (*Pcdh7*<sup>−/−</sup> and *Pcdh7*<sup>+1/+2</sup>; supplementary material Fig. S3B) and the parental R1-129 ESC line were used to generate chimeras. Eleven to thirteen ESCs were injected into the eight-cell *Rosa26* embryo (*lacZ* expression from the *Rosa26* locus; obtained by crossing *Rosa26*<sup>+/R26R</sup> mice with CMV-Cre mice) according to standard protocols. Embryos were collected between 5 and 7 days after transfer to pseudopregnant mice and stained with X-Gal (for E9.5 embryos).

### Embryo collection, staging, head morphology analysis and tamoxifen injection

Embryos were collected at the required gestational age or at specific time points after tamoxifen or mock treatment. Embryos were staged by morphology (Downs and Davies, 1993) or somite number. The morphology of E8.5–E10.5 mutant embryos was compared with stage-matched control

embryos with specific attention to embryo and head size, number of somites and morphology of the head. Embryos were assigned to one of five categories based on the size of the forebrain and midbrain (see Fig. 4D). Tamoxifen (Sigma-Aldrich) was administered to pregnant mice by intraperitoneal injection of 1 mg (100 µl of 10 mg/ml in canola oil) per 20 g body weight. For the mock control, an equivalent volume of canola oil was administered.

### In situ hybridisation, immunostaining, X-Gal staining and histology

These followed standard protocols; details are provided in the supplementary Materials and Methods.

### Cell labelling and embryo culture experiments

Embryos were collected at mid-streak stage. Cells in the endoderm layer associated with the anterior and the posterior segment of the primitive streak were labelled with CM-Dil and DiO (Molecular Probes), respectively (Fossat et al., 2011a). Embryos were cultured *in vitro* for 24 h (Fossat et al., 2011a). Embryos were imaged under bright-field and fluorescent light (merged image) using a Leica SP5 confocal microscope before and after culture.

### Cell transfection assays for RT-qPCR and ChIP-PCR

P19 cells were transfected with different combinations of pGFP, a mock plasmid, pLhx1-HA, pLhx1Δ-HA, pLdb1 and/or pSshp3 in equimolar quantity (see supplementary Materials and Methods for details) and sorted by flow cytometry using a BD FACS Aria III cell sorter.

### Molecular cloning and luciferase assay

The generation of expression vectors and plasmids for the luciferase assay is described in the supplementary Materials and Methods. P19 cells were transfected with pGL3-promoter (empty or containing a genomic region), a pRL vector and different combinations of mock plasmid, pLhx1-HA, pLhx1Δ-HA, pLdb1 and/or pSshp3 in equimolar quantity (see supplementary Materials and Methods for details). The luciferase assay was performed as described previously (Ip et al., 2014).

### Sampling for RT-qPCR analysis

The following were sampled for RT-qPCR analysis: 15 Lhx1-epiCKO (*Lhx1*<sup>fl/fl</sup>, *Meox2*<sup>+/-Cre</sup>) and 15 control (*Lhx1*<sup>+/+</sup>, *Meox2*<sup>+/-Cre</sup>) stage-matched (early-bud to head-fold) E7.75 embryos; five Lhx1-ameCKO (*Lhx1*<sup>fl/fl</sup>, *Foxa2*<sup>+/-mcm</sup>) and five control (*Lhx1*<sup>fl/fl</sup>, *Foxa2*<sup>+/+</sup> or *Lhx1*<sup>fl/fl</sup>, *Foxa2*<sup>+/-mcm</sup>) stage-matched (neural groove to head-fold) E7.75 embryos 32±2 h after tamoxifen injection at E6.5; five *Lhx1*<sup>+/-</sup>, *Dkk1*<sup>+/-</sup>, three *Lhx1*<sup>+/-</sup>, five *Dkk1*<sup>+/-</sup> and five wild-type stage-matched (early-bud to head-fold) E7.75 embryos. Each embryo was bisected longitudinally to isolate anterior germ layer tissues for analysis.

For cell experiments, flow-sorted GFP-expressing cells were collected in triplicate for each condition of transfection.

RNA isolation and RT-qPCR conditions are described in the supplementary Materials and Methods.

### ChIP-PCR analysis

The EZ-Magna ChIP Kit (Millipore) was used (see supplementary Materials and Methods for details). For *Pcdh7*, a previously established ChIP-qPCR protocol was used (Ip et al., 2014). Primer sequences were as published (Ip et al., 2014) or are listed in supplementary material Table S6.

### Acknowledgements

We thank Xin Wang for help with flow cytometry; Laurence Cantrell for assistance with microscopy; and the CMRI Bioservices unit for animal care.

### Competing interests

The authors declare no competing or financial interests.

### Author contributions

N.F., C.K.I., V.J.J., J.B.S., P.-L.K., S.L.L., M.P. and K.T. performed the experiments. D.A.F.L. performed preliminary experiments. K.M.K. and R.R.B. provided the experimental materials. N.F., C.K.I. and P.P.L.T. designed the experiments, analysed the data and prepared the manuscript for publication.

### Funding

Our work was supported by the National Health and Medical Research Council (NHMRC) of Australia [grant 632777] and Mr James Fairfax. N.F. was a University of Sydney Post-Doctoral Fellow and holds the Sir Norman Gregg Research Fellowship of CMRI. C.K.I. was supported by an International Postgraduate Scholarship and an International Australian Postgraduate Scholarship of the University of Sydney. P.P.L.T. is an NHMRC Senior Principal Research Fellow [grant 1003100]. The Flow Cytometry Centre is supported by Westmead Millennium Institute, NHMRC and Cancer Institute, NSW. The Leica SP5 in the CLEM Suite at KRI was supported by the following grants: Cancer Institute NSW Research Equipment [10/REG/1-23], NHMRC [2009-02759], the Ian Potter Foundation [20100508], the Perpetual Foundation [730], Ramaciotti Foundation [3037/2010] and the Sydney Medical School Research Infrastructure Major Equipment Scheme.

### Supplementary material

Supplementary material available online at <http://dev.biologists.org/lookup/suppl/doi:10.1242/dev.120907/-DC1>

### References

- Andoniadou, C. L., Signore, M., Sajedi, E., Gaston-Massuet, C., Kelberman, D., Burns, A. J., Itasaki, N., Dattani, M. and Martinez-Barbera, J. P. (2007). Lack of the murine homeobox gene Hesx1 leads to a posterior transformation of the anterior forebrain. *Development* **134**, 1499–1508.
- Andoniadou, C. L., Signore, M., Young, R. M., Gaston-Massuet, C., Wilson, S. W., Fuchs, E. and Martinez-Barbera, J. P. (2011). HESX1- and TCF3-mediated repression of Wnt/beta-catenin targets is required for normal development of the anterior forebrain. *Development* **138**, 4931–4942.
- Arkell, R. M. and Tam, P. P. L. (2012). Initiating head development in mouse embryos: integrating signalling and transcriptional activity. *Open Biol.* **2**, 120030.
- Arkell, R. M., Fossat, N. and Tam, P. P. L. (2013). Wnt signalling in mouse gastrulation and anterior development: new players in the pathway and signal output. *Curr. Opin. Genet. Dev.* **23**, 454–460.
- Bildsoe, H., Loebel, D. A. F., Jones, V. J., Hor, A. C. C., Braithwaite, A. W., Chen, Y.-T., Behringer, R. R. and Tam, P. P. L. (2013). The mesenchymal architecture of the cranial mesoderm of mouse embryos is disrupted by the loss of Twist1 function. *Dev. Biol.* **374**, 295–307.
- Bradley, R. S., Espeseth, A. and Kintner, C. (1998). NF-protocadherin, a novel member of the cadherin superfamily, is required for Xenopus ectodermal differentiation. *Curr. Biol.* **8**, 325–334.
- Burtscher, I. and Lickert, H. (2009). Foxa2 regulates polarity and epithelialization in the endoderm germ layer of the mouse embryo. *Development* **136**, 1029–1038.
- Camus, A., Davidson, B. P., Billiards, S., Khoo, P., Rivera-Perez, J. A., Wakamiya, M., Behringer, R. R. and Tam, P. P. (2000). The morphogenetic role of midline mesendoderm and ectoderm in the development of the forebrain and the midbrain of the mouse embryo. *Development* **127**, 1799–1813.
- Chou, S.-J., Hermesz, E., Hatta, T., Feitner, D., El-Hodiri, H. M., Jamrich, M. and Mahon, K. (2006). Conserved regulatory elements establish the dynamic expression of Rpx/Hesxl in early vertebrate development. *Dev. Biol.* **292**, 533–545.
- Downs, K. M. and Davies, T. (1993). Staging of gastrulating mouse embryos by morphological landmarks in the dissecting microscope. *Development* **118**, 1255–1266.
- Enkmandakh, B., Makeyev, A. V. and Bayarsaikhan, D. (2006). The role of the proline-rich domain of Ssdp1 in the modular architecture of the vertebrate head organizer. *Proc. Natl. Acad. Sci. USA* **103**, 11631–11636.
- Flicek, P., Ahmed, I., Amode, M. R., Barrell, D., Beal, K., Brent, S., Carvalho-Silva, D., Clapham, P., Coates, G., Fairley, S. et al. (2013). Ensembl 2013. *Nucleic Acids Res.* **41**, D48–D55.
- Fossat, N., Loebel, D. A. F., Jones, V., Khoo, P. L., Bildsoe, H. and Tam, P. P. L. (2011a). Approaches for tracking cell behaviour and the impact of experimentally altered gene activity in mouse embryos. In *Optical Imaging in Developmental Biology: A Laboratory Manual* (ed. R. Wong and J. Sharpe), pp. 311–329. Cold Spring Harbor, New York: Cold Spring Harbor Laboratory Press.
- Fossat, N., Jones, V., Khoo, P. L., Bogani, D., Hardy, A., Steiner, K., Mukhopadhyay, M., Westphal, H., Nolan, P. M., Arkell, R. et al. (2011b). Stringent requirement of a proper level of canonical WNT signalling activity for head formation in mouse embryo. *Development* **138**, 667–676.
- Fossat, N., Jones, V., Garcia-Garcia, M. J. and Tam, P. P. L. (2012). Modulation of WNT signaling activity is key to the formation of the embryonic head. *Cell Cycle* **11**, 26–32.
- Hikasa, H. and Sokol, S. Y. (2013). Wnt signaling in vertebrate axis specification. *Cold Spring Harb. Perspect. Biol.* **5**, a007955.
- Robert, O. and Westphal, H. (2000). Functions of LIM-homeobox genes. *Trends Genet.* **16**, 75–83.
- Hukriede, N. A., Tsang, T. E., Habas, R., Khoo, P. L., Steiner, K., Weeks, D. L., Tam, P. P. L. and Dawid, I. B. (2003). Conserved requirement of Lim1 function for cell movements during gastrulation. *Dev. Cell* **4**, 83–94.

- Ip, C. K., Fossat, N., Jones, V., Lamonerie, T. and Tam, P. P. L.** (2014). Head formation: OTX2 regulates Dkk1 and Lhx1 activity in the anterior mesendoderm. *Development* **141**, 3859-3867.
- Iwafuchi-Doi, M., Matsuda, K., Murakami, K., Niwa, H., Tesar, P. J., Aruga, J., Matsuo, I. and Kondoh, H.** (2012). Transcriptional regulatory networks in epiblast cells and during anterior neural plate development as modeled in epiblast stem cells. *Development* **139**, 3926-3937.
- Kemp, C., Willems, E., Abdo, S., Lambiv, L. and Leyns, L.** (2005). Expression of all Wnt genes and their secreted antagonists during mouse blastocyst and postimplantation development. *Dev. Dyn.* **233**, 1064-1075.
- Kiecker, C. and Niehrs, C.** (2001). A morphogen gradient of Wnt/beta-catenin signalling regulates anteroposterior neural patterning in *Xenopus*. *Development* **128**, 4189-4201.
- Kimura-Yoshida, C., Nakano, H., Okamura, D., Nakao, K., Yonemura, S., Belo, J. A., Aizawa, S., Matsui, Y. and Matsuo, I.** (2005). Canonical Wnt signaling and its antagonist regulate anterior-posterior axis polarization by guiding cell migration in mouse visceral endoderm. *Dev. Cell* **9**, 639-650.
- Kwan, K. M. and Behringer, R. R.** (2002). Conditional inactivation of Lim1 function. *Genesis* **32**, 118-120.
- Lagutin, O. V., Zhu, C. C., Kobayashi, D., Topczewski, J., Shimamura, K., Puelles, L., Russell, H. R. C., McKinnon, P. J., Solnica-Krezel, L. and Oliver, G.** (2003). Six3 repression of Wnt signaling in the anterior neuroectoderm is essential for vertebrate forebrain development. *Genes Dev.* **17**, 368-379.
- Lewis, S. L., Khoo, P.-L., Andrea De Young, R., Bildsoe, H., Wakamiya, M., Behringer, R. R., Mukhopadhyay, M., Westphal, H. and Tam, P. P. L.** (2007). Genetic interaction of Gsc and Dkk1 in head morphogenesis of the mouse. *Mech. Dev.* **124**, 157-165.
- Lewis, S. L., Khoo, P.-L., De Young, R. A., Steiner, K., Wilcock, C., Mukhopadhyay, M., Westphal, H., Jamieson, R. V., Robb, L. and Tam, P. P. L.** (2008). Dkk1 and Wnt3 interact to control head morphogenesis in the mouse. *Development* **135**, 1791-1801.
- Li, A.-M., Tian, A.-X., Zhang, R.-X., Ge, J., Sun, X. and Cao, X.-C.** (2013). Protocadherin-7 induces bone metastasis of breast cancer. *Biochem. Biophys. Res. Commun.* **436**, 486-490.
- Maretti, S., Cordenonsi, M., Dupont, S., Braghetta, P., Broccoli, V., Hassan, A. B., Volpin, D., Bressan, G. M. and Piccolo, S.** (2003). Mapping Wnt/beta-catenin signaling during mouse development and in colorectal tumors. *Proc. Natl. Acad. Sci. USA* **100**, 3299-3304.
- Martinez-Barbera, J. P., Rodriguez, T. A. and Beddington, R. S. P.** (2000). The homeobox gene Hesx1 is required in the anterior neural ectoderm for normal forebrain formation. *Dev. Biol.* **223**, 422-430.
- Mochizuki, T., Karavanov, A. A., Curtiss, P. E., Ault, K. T., Sugimoto, N., Watabe, T., Shiokawa, K., Jamrich, M., Cho, K. W. Y., Dawid, I. B. et al.** (2000). Xlim-1 and LIM domain binding protein 1 cooperate with various transcription factors in the regulation of the goosecoid promoter. *Dev. Biol.* **224**, 470-485.
- Morishita, H. and Yagi, T.** (2007). Protocadherin family: diversity, structure, and function. *Curr. Opin. Cell Biol.* **19**, 584-592.
- Mukhopadhyay, M., Shtrom, S., Rodriguez-Esteban, C., Chen, L., Tsukui, T., Gomer, L., Dorward, D. W., Glinka, A., Grinberg, A., Huang, S.-P. et al.** (2001). Dickkopf1 is required for embryonic head induction and limb morphogenesis in the mouse. *Dev. Cell* **1**, 423-434.
- Mukhopadhyay, M., Teufel, A., Yamashita, T., Agulnick, A. D., Chen, L., Downs, K. M., Schindler, A., Grinberg, A., Huang, S.-P., Dorward, D. et al.** (2003). Functional ablation of the mouse Ldb1 gene results in severe patterning defects during gastrulation. *Development* **130**, 495-505.
- Nakano, T., Murata, T., Matsuo, I. and Aizawa, S.** (2000). OTX2 directly interacts with LIM1 and HNF-3beta. *Biochem. Biophys. Res. Commun.* **267**, 64-70.
- Nishioka, N., Nagano, S., Nakayama, R., Kiyonari, H., Ijiri, T., Taniguchi, K., Shawlot, W., Hayashizaki, Y., Westphal, H., Behringer, R. R. et al.** (2005). Ssdp1 regulates head morphogenesis of mouse embryos by activating the Lim1-Ldb1 complex. *Development* **132**, 2535-2546.
- Park, E. J., Sun, X., Nichol, P., Saijoh, Y., Martin, J. F. and Moon, A. M.** (2008). System for tamoxifen-inducible expression of cre-recombinase from the Foxa2 locus in mice. *Dev. Dyn.* **237**, 447-453.
- Petersen, C. P. and Reddien, P. W.** (2009). Wnt signaling and the polarity of the primary body axis. *Cell* **139**, 1056-1068.
- Pfister, S., Steiner, K. A. and Tam, P. P. L.** (2007). Gene expression pattern and progression of embryogenesis in the immediate post-implantation period of mouse development. *Gene Expr. Patterns* **7**, 558-573.
- Piccolo, S., Agius, E., Leyns, L., Bhattacharyya, S., Grunz, H., Bouwmeester, T. and De Robertis, E. M.** (1999). The head inducer Cerberus is a multifunctional antagonist of Nodal, BMP and Wnt signals. *Nature* **397**, 707-710.
- Ran, F. A., Hsu, P. D., Wright, J., Agarwala, V., Scott, D. A. and Zhang, F.** (2013). Genome engineering using the CRISPR-Cas9 system. *Nat. Protoc.* **8**, 2281-2308.
- Rashid, D., Newell, K., Shama, L. and Bradley, R.** (2006). A requirement for NF-protocadherin and TAF1/Set in cell adhesion and neural tube formation. *Dev. Biol.* **291**, 170-181.
- Saga, Y., Miyagawa-Tomita, S., Takagi, A., Kitajima, S., Miyazaki, J. and Inoue, T.** (1999). MesP1 is expressed in the heart precursor cells and required for the formation of a single heart tube. *Development* **126**, 3437-3447.
- Schwenk, F., Baron, U. and Rajewsky, K.** (1995). A cre-transgenic mouse strain for the ubiquitous deletion of loxP-flanked gene segments including deletion in germ cells. *Nucleic Acids Res.* **23**, 5080-5081.
- Shawlot, W. and Behringer, R. R.** (1995). Requirement for Lim1 in head-organizer function. *Nature* **374**, 425-430.
- Shawlot, W., Wakamiya, M., Kwan, K. M., Kania, A., Jessell, T. M. and Behringer, R. R.** (1999). Lim1 is required in both primitive streak-derived tissues and visceral endoderm for head formation in the mouse. *Development* **126**, 4925-4932.
- Shawlot, W., Min Deng, J., Wakamiya, M. and Behringer, R. R.** (2000). The cerberus-related gene, Cerr1, is not essential for mouse head formation. *Genesis* **26**, 253-258.
- Shimono, A. and Behringer, R. R.** (1999). Isolation of novel cDNAs by subtractions between the anterior mesendoderm of single mouse gastrula stage embryos. *Dev. Biol.* **209**, 369-380.
- Shimono, A. and Behringer, R. R.** (2003). Angiomotin regulates visceral endoderm movements during mouse embryogenesis. *Curr. Biol.* **13**, 613-617.
- Soriano, P.** (1999). Generalized lacZ expression with the ROSA26 Cre reporter strain. *Nat. Genet.* **21**, 70-71.
- Spieler, D., Bäumer, N., Stebler, J., Köprunner, M., Reichman-Fried, M., Teichmann, U., Raz, E., Kessel, M. and Wittler, L.** (2004). Involvement of Pax6 and Otx2 in the forebrain-specific regulation of the vertebrate homeobox gene ANF/Hesx1. *Dev. Biol.* **269**, 567-579.
- Sudou, N., Yamamoto, S., Ogino, H. and Taira, M.** (2012). Dynamic in vivo binding of transcription factors to cis-regulatory modules of cer and gsc in the stepwise formation of the Spemann-Mangold organizer. *Development* **139**, 1651-1661.
- Tallquist, M. D. and Soriano, P.** (2000). Epiblast-restricted Cre expression in MORE mice: a tool to distinguish embryonic vs. extra-embryonic gene function. *Genesis* **26**, 113-115.
- Tam, P. P. L., Khoo, P.-L., Lewis, S. L., Bildsoe, H., Wong, N., Tsang, T. E., Gad, J. M. and Robb, L.** (2007). Sequential allocation and global pattern of movement of the definitive endoderm in the mouse embryo during gastrulation. *Development* **134**, 251-260.
- Tanaka, S. S., Yamaguchi, Y. L., Steiner, K. A., Nakano, T., Nishinakamura, R., Kwan, K. M., Behringer, R. R. and Tam, P. P. L.** (2010). Loss of Lhx1 activity impacts on the localization of primordial germ cells in the mouse. *Dev. Dyn.* **239**, 2851-2859.
- van Amerongen, R. and Nusse, R.** (2009). Towards an integrated view of Wnt signaling in development. *Development* **136**, 3205-3214.
- Viotti, M., Nowotschin, S. and Hadjantonakis, A.-K.** (2014). SOX17 links gut endoderm morphogenesis and germ layer segregation. *Nat. Cell Biol.* **16**, 1146-1156.
- Yamamoto, A., Kemp, C., Bachiller, D., Geissert, D. and De Robertis, E. M.** (2000). Mouse paraxial protocadherin is expressed in trunk mesoderm and is not essential for mouse development. *Genesis* **27**, 49-57.
- Yao, J. and Kessler, D. S.** (2001). Goosecoid promotes head organizer activity by direct repression of Xwnt8 in Spemann's organizer. *Development* **128**, 2975-2987.
- Yasuoka, Y., Suzuki, Y., Takahashi, S., Someya, H., Sudou, N., Haramoto, Y., Cho, K. W., Asashima, M., Sugano, S. and Taira, M.** (2014). Occupancy of tissue-specific cis-regulatory modules by Otx2 and TLE/Groucho for embryonic head specification. *Nat. Commun.* **5**, 4322.
- Yoshida, K.** (2003). Fibroblast cell shape and adhesion in vitro is altered by overexpression of the 7a and 7b isoforms of protocadherin 7, but not the 7c isoform. *Cell. Mol. Biol. Lett.* **8**, 735-741.
- Zorn, A. M.** (2001). Wnt signalling: antagonistic Dickkopfs. *Curr. Biol.* **11**, R592-R595.

## SUPPLEMENTARY MATERIALS AND METHODS

### In situ hybridization, Immunostaining, X-Gal staining and histology

In situ hybridization analysis of gene expression was performed using a protocol and digoxigenin-UTP cRNA probes that were previously described (Tam and Steiner, 1999; Hukriede et al., 2003; Fossat et al., 2007; Lewis et al., 2007; Fossat et al., 2011). Riboprobes for *Pcdh7* and *Pcdh19* were synthesized with T7 polymerase using fragments amplified by PCR from cDNA of mouse embryoid bodies with the following primers: *Pcdh7*: 5'-CCCACTCACCCAGGATATA and 5'-ATCGTAATACGACTCACTATAGGGTACTCGGAGCAGTGATCT; *Pcdh19*: 5'-CCACCAAGCCTCTATATCT and 5'-ATCGTAATACGACTCACTATAGGGCACAACTGAATTGCCTCTG.

Wholemount immunostaining adapted from (Burtscher and Lickert, 2009) was performed using primary antibodies against FOXA2 (1:1000; SC-6554; Santa Cruz Biotechnology) and E-Cadherin (1:300; 13-1900; Invitrogen). Embryo were also stained with DAPI (1:1000) and imaged (in separate channels) with a Leica SP5 confocal microscope.

X-Gal staining was performed as previously described (Lewis et al., 2007; Fossat et al., 2011). For histology, stained embryos were embedded in paraffin wax, sectioned and counter-stained with nuclear fast-red (Tam and Steiner, 1999; Lewis et al., 2007).

At least 3 specimens of each genotype were analysed for each staining.

### Molecular cloning

The following mouse coding sequences were amplified by PCR from E7.5 embryos cDNA using the primers described below and cloned between the Sall and NotI sites of the pCMV-SPORT6 plasmid (Invitrogen) (*Ldb1*, *Ssbp3*) or between the Sall and XbaI sites of a pCMV-SPORT6 plasmid containing a HA tag coding sequence (primers 5'-CTAGATAACCATACTGACGTTCCAGACTACGCTTAGC and 5'-TCGAGCTAACGCTAGTCTGGAACGTCGTATGGGTAT cloned between the XbaI and Xhol sites) (*Lhx1* and

*Lhx1Δ*): (i) *Ldb1*: 5'-GATCGTCGACACCATGCTGGATCGGGATGTGG and 5'-GATCGCGGCCGCTACTTATCGTCGTCATCCTGTAATCCTGGGAAGCCTGTGACGTG; (ii) *Ssbp3*: 5'-GATCGTCGACACCATGTTGCCAAA GGCAAAGG and 5'-GATCGCGGCCGCTACGTAGAATCGAGACCGAGGGAGAGGGTAGGGATAGGCTTACCC ACGCTCATCGTCATGCTC; (iii) *Lhx1*: 5'-GATCGTCGACACCATGGTGCACTGTGCGGGC and 5'-GATCTCTAG ACCACACGGCTGCCTCGTT; (iv) *Lhx1Δ* (Last ~500 bp of mouse *Lhx1* coding sequences that do not contain the DNA and the protein binding domains): 5'-GATCGTCGACACCATGAAACAGCTAACCGCG CTAG and 5'-GATCTCTAGACCACACGGCTGCCTCGTT.

Vectors for luciferase assay: Genomic regions were amplified by PCR from mouse genomic DNA with primers described below and cloned into the Xhol site or between the NheI and the KpnI sites of the pGL3-promoter plasmid (Promega): (i) *Pcdh7* -0.2R: 5'-ATCGGGTACCGCGGCTGAGAATCCAAACTT and 5'-ATCGGCTAGCTCCTGCTTCTTCGAAAGTT; (ii) *Pcdh7* +8.5R: 5'-ATCGCTCGAGGCAGTGTGGAGA and 5'-ATCGCTCGAGACACTCAACCACAATGCTGA; (iii) Wild type or (iv) mutated dH1: 5'-ATCGCTCGAGCGAGGTTGATTGGGATCA and 5'-ATCGCTCGAGCACATGAGATCAAAGTGGCT. In the case of mutated dH1 where LHX1 binding site YTAATNN (Mochizuki et al., 2000; Sudou et al., 2012; Yasuoka et al., 2014) is mutated into YGCGCNN, fragment was amplified from two PCR products pooled and previously amplified with primers set 5'-ATCGCTCGAGCGAGGTTGATTGGGATCA and 5'-CTTCTCGCGCGTGTTCATATCGCTGAGCA and primers set 5'-TGAAACACGCGCGAGAAAGCCGGGAGCTAAG and 5'-ATCGCTCGAGCACATGAGATCAAAGTGGCT.

The sequence of the cloned fragments was verified by Sanger sequencing.

#### Cell transfection assays for RT-PCR and ChIP-PCR

Embryonal carcinoma P19 cells (in 10-cm dish) were transfected using Fugene 6 (Roche) with: (i) pGFP (pNF-5; (Fossat et al., 2014)) (1 µg) + mock plasmid (9 µg), (ii) pGFP (1 µg) + pLhx1-HA (3 µg) + mock plasmid (6 µg), (iii) pGFP (1 µg) + pLdb1 (3 µg) + pSsbp3 (3 µg) + mock plasmid (3 µg), (iv) pGFP (1 µg) + pLhx1-HA (3 µg) + pLdb1 (3 µg) + pSsbp3 (3 µg) or (v) pGFP (1 µg) + pLhx1Δ-HA (3 µg) +

pLdb1 (3 µg) + pSsbp3 (3 µg). The mock plasmid is a pCMV-SPORT6 expressing a non-functional form of RBM47 that does not have any activity on head formation (Fossat et al., 2014). 24 h after transfection, GFP-expressing cells were sorted by flow cytometry and snap-frozen for storage until further analysis. Samples for ChIP-PCR analysis were treated with paraformaldehyde (for cross-linking) prior to storage.

### **Luciferase assay**

Embryonal carcinoma P19 cells (in 1.5 cm well) were transfected using Fugene 6 (Roche) with pGL3-promoter only or pGL3-promoter containing either *Pcdh7* -0.2R, *Pcdh7* +8.5R, *Dkk1* dH1 or *Dkk1* mutated dH1 (0.25 µg) and (i) mock plasmid (0.75 µg), (ii) mock plasmid (0.50 µg) + pLhx1-HA (0.25 µg), (iii) mock plasmid (0.50 µg) + pLhx1Δ-HA (0.25 µg), (iv) mock plasmid (0.25 µg) + pLdb1 (0.25 µg) + pSsbp3 (0.25 µg) or (v) pLdb1 (0.25 µg) + pSsbp3 (0.25 µg) + pLhx1-HA (0.25 µg). Cells were co-transfected with pRL renilla luciferase reporter vector (25 ng; Promega). Cells were collected 24 h after transfection, and luciferase assay was performed as described before (Ip et al., 2014) on three independent samples from each transfection experiment. Firefly luciferase activity was normalised against renilla luciferase activity.

### **RNA isolation and RT-qPCR**

For the *Lhx1*-epiCKO study, three independent pools of five anterior fragments of mutant and control E7.75 embryos were analysed independently. For the *Lhx1*-ameCKO and the *Lhx1;Dkk1* study, anterior fragments of the E7.75 embryos (three or five per genotype) were analysed independently. For cell experiments, each replicate of flow-sorted GFP-expressing cells was analysed independently. Total RNA was extracted using the RNeasy Micro Kit (Qiagen). cDNAs were synthesized from 5-10 ng (individual embryos), 30-40 ng (pooled embryo fragments) or 100 ng (GFP cells) of total RNA using the Superscript III First Strand System (Invitrogen). Quantitative PCR was

performed in technical triplicate and normalised against *β-Actin* using protocol and primers described before (Fossat et al., 2011) or listed in Supplementary **Table S6A**.

#### **ChIP-PCR analysis**

Cells were cross-linked with 37% formaldehyde and sonicated to generate genomic DNA fragments of 200 to 1000 bp sizes. 20 µl of the fragmented chromatin was collected for the input. 50 µl (about one third of the chromatin obtained from 250000 cells) was incubated with rabbit polyclonal HA antibody (Santa Cruz, sc-805) overnight at 4°C with constant rotation. Cross-linking was reversed with protease K treatment (10 µg/µL) at 62°C overnight. Immuno-precipitated chromatin and input DNA were extracted in 20 µl water using phenol-chloroform purification protocol. PCR reaction was performed on 1 µl of DNA sample using Biomix Red (Bioline) Taq polymerase. Conditions were the same for all the PCRs: 94°C for 30 seconds, 60°C for 30 seconds, 72°C for 30 seconds for 35 cycles.

**SUPPLEMENTARY FIGURES**

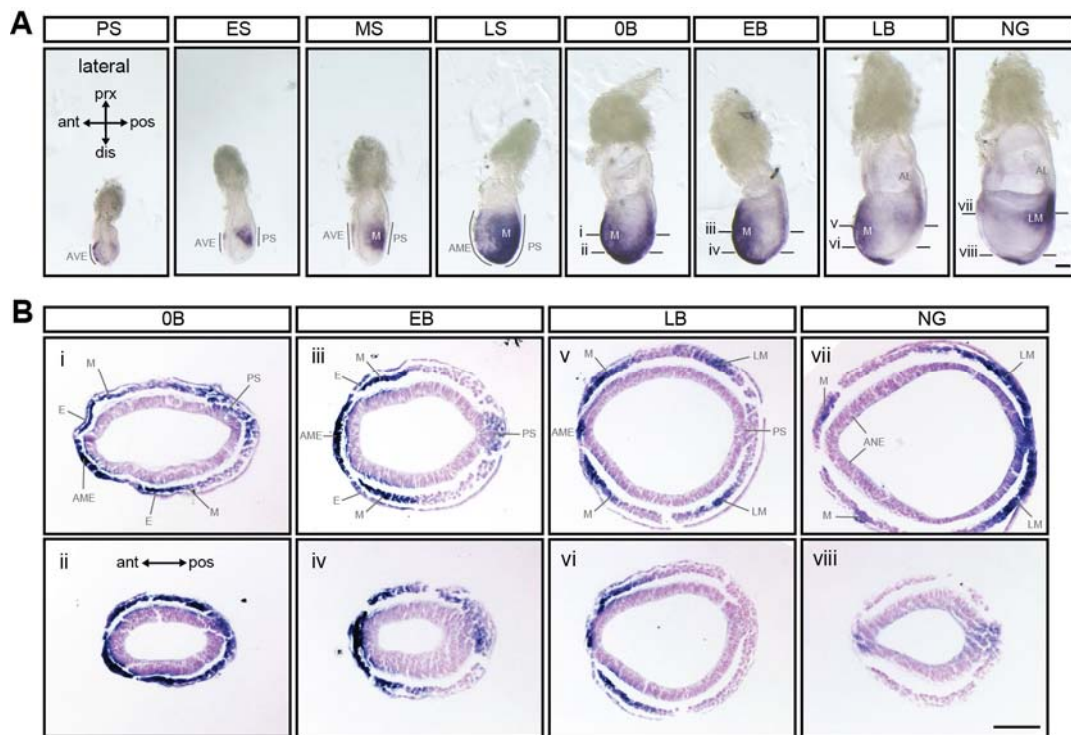


**Figure S1. *Lhx1* expression pattern.** (A) *Lhx1* whole mount *in situ* hybridization of wild type embryos at pre-streak (PS), early-streak (ES), mid-streak (MS), late-streak (LS), no-bud (OB), early-bud (EB), late-bud (LB) and neural-groove (NG) stages. (B) Histology of no-bud (OB), early-bud (EB), late-bud (LB) and neural-groove (NG) embryos shown part A. Plane of sectioning is indicated in A. AL, allantois; AME, anterior mesendoderm; ANE, anterior neurectoderm; ant, anterior; AVE, anterior visceral endoderm; dis, distal; E, endoderm; LM, lateral mesoderm; M, mesoderm; pos, posterior; prx, proximal; PS, primitive streak. Scale bars: 100 µm.

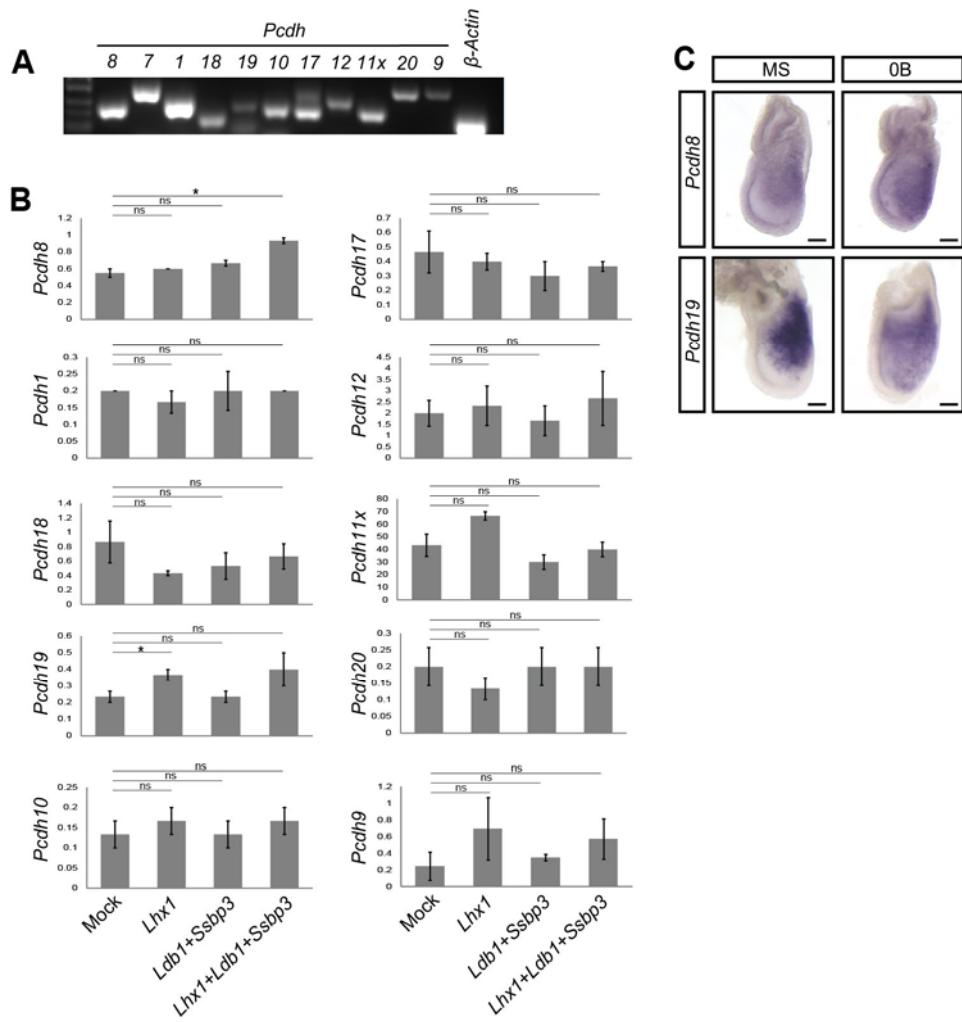


**Figure S2. Expression of the *Pcdh* genes.** (A) Expression of *Pcdh* gene family members (*Pcdh-1*, *-7*, *-8*, *-9*, *-10*, *-11x*, *-12*, *-17*, *-18*, *-19* and *-20*) relative to  $\beta$ -Actin in E7.75 mouse embryo analysed by RT-PCR. (B) Expression of *Pcdh* genes (relative to  $\beta$ -Actin) analyzed by RT-qPCR in P19 cells transfected with different combinations of vectors expressing a mock protein, *Lhx1*, *Ldb1* and/or *Ssbp3*. Data represent the mean  $\pm$  standard errors of  $N = 3$  independent experiments for each condition of transfection.  $P$ -value (\*)  $< 0.05$  and not significant (ns) by t-test. (C) Expression of *Pcdh8* and *Pcdh19* in the mesoderm but not in the anterior mesendoderm of the mid-streak (MS) and no-bud (OB) stage embryo. Lateral view of specimens with anterior to the left. Scale bars: 100  $\mu$ m.

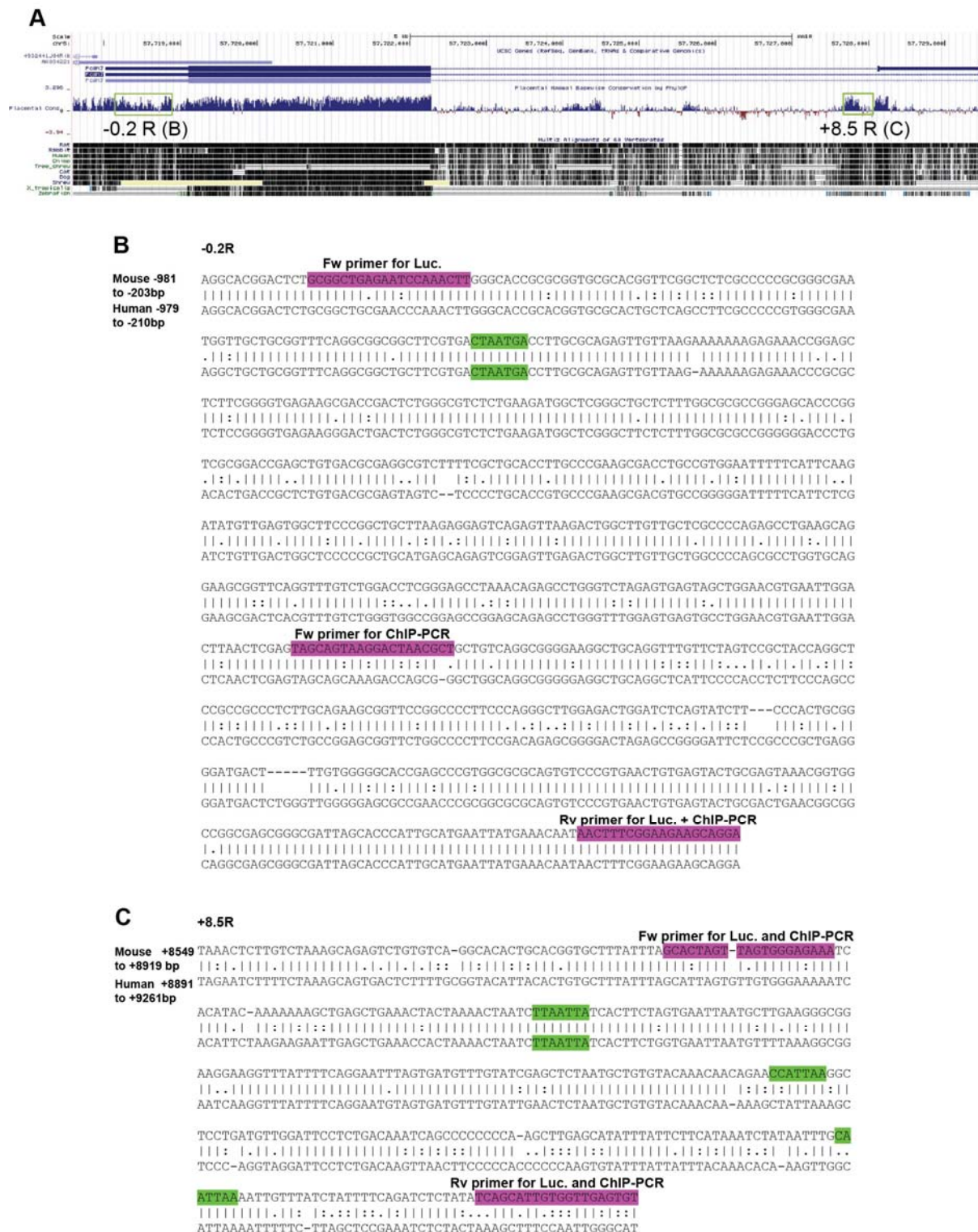


**Figure S3. Mouse *Pcdh7* -0.2R and +8.5R regions. (A)** Genomic information of the *Pcdh7* locus in sense orientation (UCSC genomic browser). Thick blue boxes indicate coding sequences and thin blue boxes indicate untranslated regions. Placental mammal base-wise conservation (Placental Cons) is shown below the track. Two regions are highlighted: -0.2 R (B) and +8.5 R (C). **(B)** Sequences of primers used for luciferase reporter assay and ChIP-PCR. **(C)** Sequences of primers used for luciferase reporter assay and ChIP-PCR.

histogram shows the result of multiple sequence alignment for 60 vertebrate species. The conservation score was measured by phyloP. The blue bar indicates positive score in which the regions are conserved, whereas regions with negative score in red indicate are not conserved. Gray scale density plot display pairwise alignments for each species (Rat, Rabbit, Human, Chimp, Dog, Tree Shrew, Cat, Dog, *X tropicalis*, Zebrafish). Gray scales with darker values indicate higher level of overall conservation scored by phastCons. The green box delineates the conserved genomic location covering the -0.2R and the +8.5R regions. **(B)** Basewise sequence alignment of the mouse (-981 to -203 bp upstream of START codon) and the human (-979 to -210bp upstream of START codon) *Pcdh7* -0.2R region. **(C)** Basewise sequence alignment of the mouse (+8549 to +8919 bp downstream of START codon) and the human (+8891 to +9261bp downstream of START codon) *Pcdh7* +8.5R region. Sequences of the primers used for ChIP-qPCR and luciferase (Luc.) assay are highlighted in purple. Fw, forward primer; Rv, reverse primer. Sequences highlighted in green are LHX1 recognition motifs.

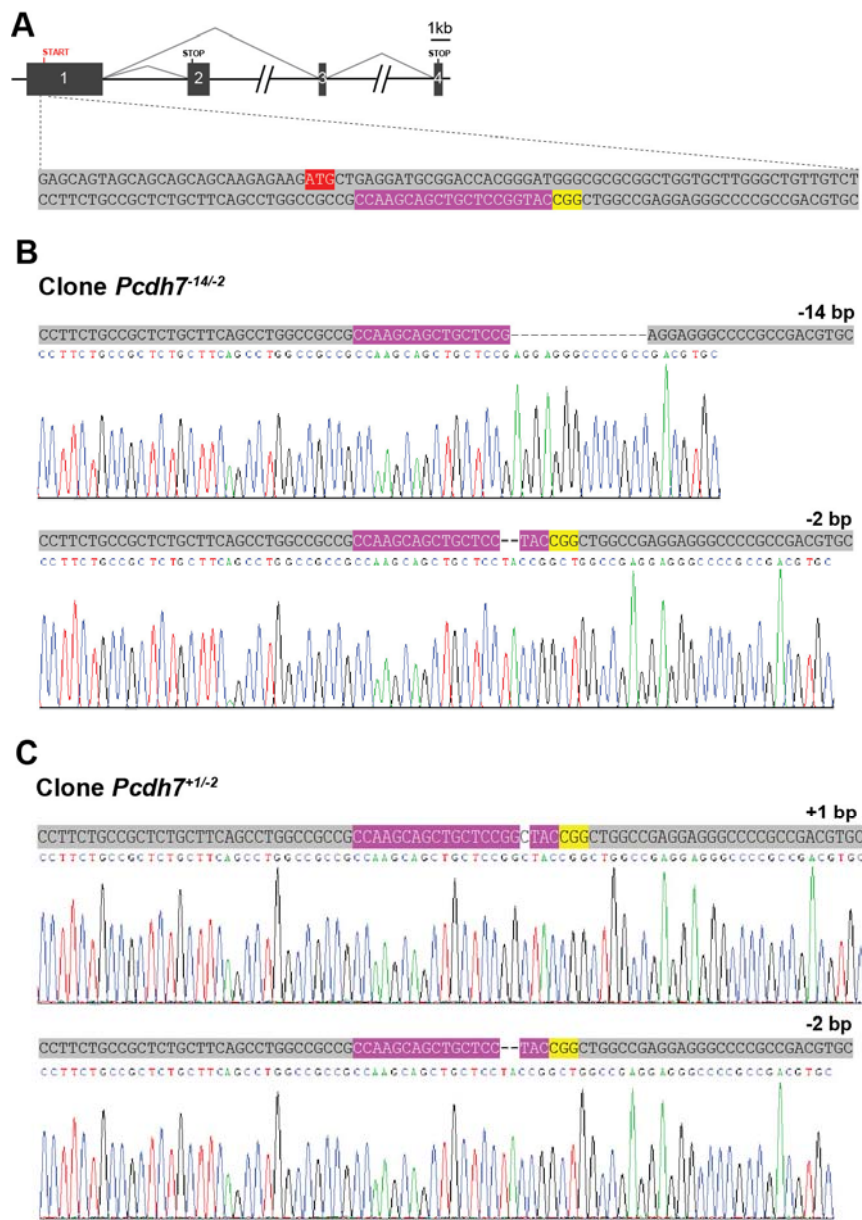


**Figure S4. Mutant *Pcdh7* alleles generated by CRISPR-Cas9 editing.** (A) Genome structure of the *Pcdh7* locus. Exons (grey boxes), splicing pattern (grey lines), START codon, STOP codon and the scale are indicated. Between dashed lines is a detailed view of the region downstream the START codon (ATG; highlighted in red) showing the sequence recognised by the sgRNA (highlighted in pink) used for experiment and the immediately adjacent PAM sequence (highlighted in yellow). (B, C) Mutant *Pcdh7* alleles of two independent ES cells clones obtained and used for the chimera experiments: (B) Clone *Pcdh7*<sup>14/-2</sup>: allele #1, 14 bp deletion; allele #2, 2 bp deletion, and (C) clone *Pcdh7*<sup>+1/-2</sup>: allele #1, 1 bp insertion; allele #2, 2 bp deletion. Sanger sequencing chromatograms are

shown for each allele. The clones have been selected for the chimera experiments based on the fact that they have bi-allelic frame shift mutations of the open reading frame of the coding sequence of *Pcdh7*.

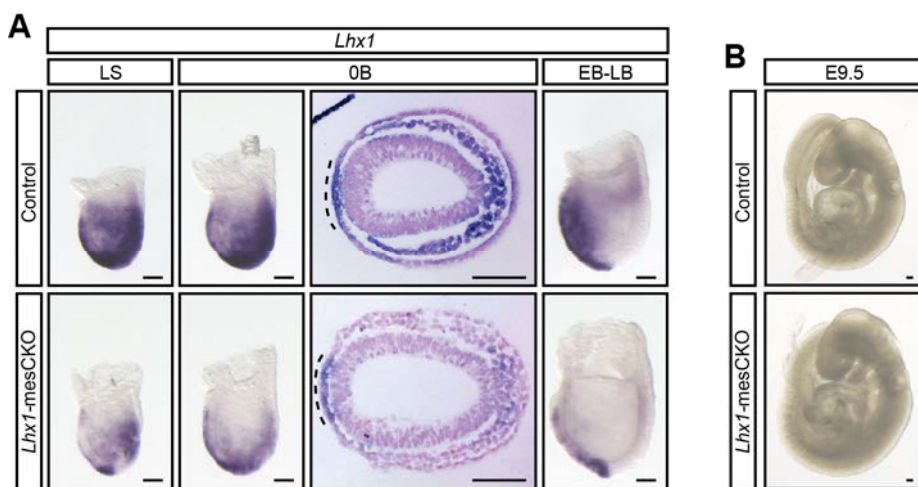
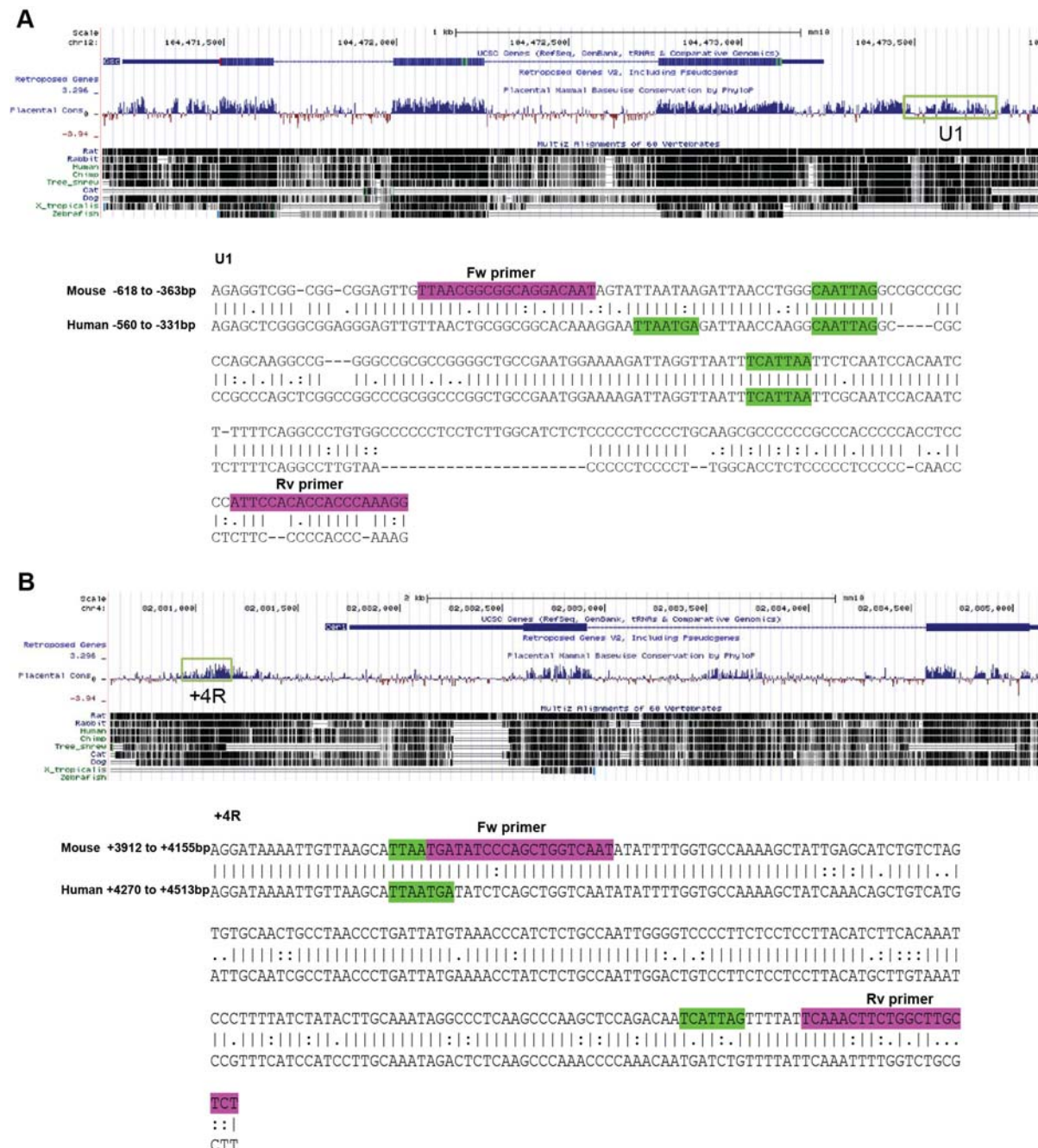


**Figure S5. Conditional deletion of *Lhx1* in the mesoderm.** (A) Detection of *Lhx1* RNA by whole mount in situ hybridization in late-streak (LS), no-bud (OB), early- to late-bud (EB-LB) control and *Lhx1*<sup>−/flox</sup>; *Mesp1*<sup>Cre</sup> (*Lhx1*-mesCKO) embryos. Transverse sections of OB-stage *Lhx1*-mesCKO embryo shows the loss of *Lhx1* expression in the mesoderm, but expression was retained in the anterior mesendoderm (dashed line) and the nascent mesenchyme in the primitive streak. (B) E9.5 control and *Lhx1*-mesCKO embryos showing similar morphology. Lateral view of whole-mount specimens and sections with anterior side to the left. The cross between *Lhx1*<sup>flox/flox</sup> and *Lhx1*<sup>+/+</sup>; *Mesp1*<sup>+/Cre</sup> mice generated embryos of four genotypes, which were present in a ratio consistent to the Mendelian distribution ( $N = 21$ , 3 litters: *Lhx1*<sup>+/flox</sup>; *Mesp1*<sup>+/+</sup>: 33%, *Lhx1*<sup>+/flox</sup>; *Mesp1*<sup>+/Cre</sup>: 24%, *Lhx1*<sup>flox/−</sup>; *Mesp1*<sup>+/+</sup>: 14% and *Lhx1*<sup>flox/−</sup>; *Mesp1*<sup>+/Cre</sup>: 29%). Scale bars: 100  $\mu$ m.



C



**Figure S6. Mouse *Gsc* U1, *Cer1* +4R and *Dkk1* H1 regions.** (A) Top: Genomic information of the mouse *Gsc* locus in antisense orientation (UCSC genomic browser). The green box delineates the conserved genomic location covering the U1 region. Bottom: Base-wise sequence alignment of the mouse (-618 to -363 bp upstream of START codon) and the human (-560 to -331bp upstream of START codon) U1 region. (B) Top: Genomic information of the mouse *Cer1* locus in antisense orientation (UCSC genomic browser). The green box delineates the conserved genomic location covering the +4R region. Bottom: Base-wise sequence alignment of the mouse (+3912 to +4155 bp downstream of START codon) and the human (+4270 to +4513bp downstream of START codon) +4R

region. **(C)** Top: Genomic information of the mouse *Dkk1* locus in antisense orientation (UCSC genomic browser). The green box delineates the conserved genomic location covering the H1 region. Bottom: Base-wise sequence alignment of the mouse (-1237 to -518 bp upstream of START codon) and the human (-1204 to -512bp upstream of START codon) H1 region {Kimura-Yoshida, 2005 #281}. Thick blue boxes indicate coding sequences and narrow blue boxes indicate untranslated regions. Placental mammal basewise conservation (Placental Cons) histogram shows the result of multiple sequence alignment for 60 vertebrate species. The conservation score was determined by phyloP. The blue bar indicates positive score for the conserved regions, whereas unconserved regions are marked with negative score in red. Gray scale density plot displays pairwise alignments for each species (Rat, Rabbit, Human, Chimp, Dog, Tree Shrew, Cat, Dog, X tropicalis, Zebrafish). Gray scales with darker values indicate higher level of overall conservation scored by phastCons. Sequences of the primers used for ChIP-PCR and luciferase assay are highlighted in purple. Fw, forward primer; Rv, reverse primer. Sequences highlighted in green are LHX1 recognition motifs.

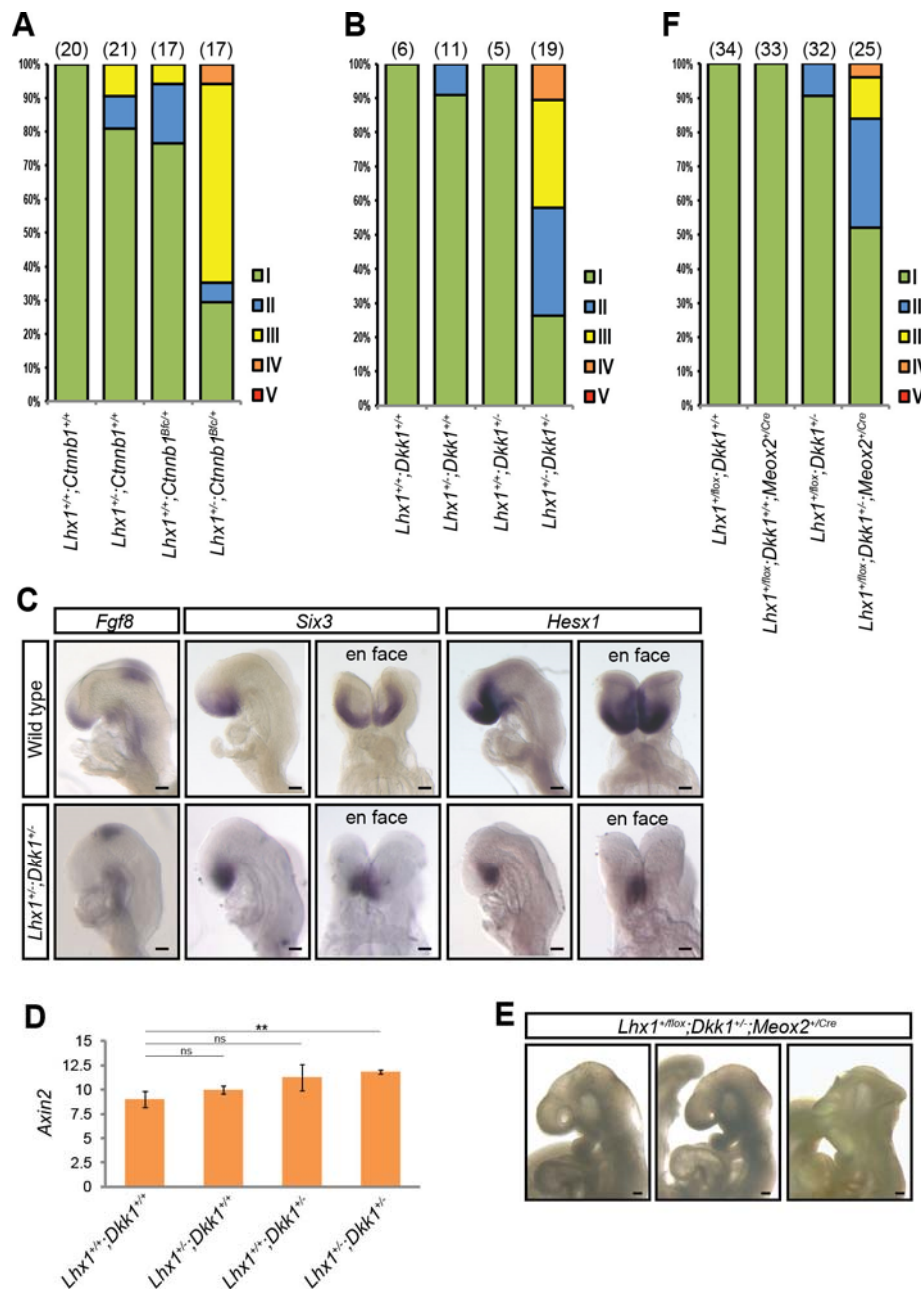


**Figure S7. Genetic interaction of *Lhx1* activity and WNT signalling.** (A, B, F) Histograms representing the distribution of the embryos of the different genotypes (X-axis) to the five head phenotype categories (colour-coded on the right). The categories are based on the size of the fore- and midbrain: [I] Normal size, [II] slight reduction ( $\leq 25\%$ ), [III] strong reduction (26-75% reduction), [IV] tissue remnant ( $> 75\%$  reduction), [V] tissues absent. The height of the bar indicates the percentage of embryos of each phenotype category. The number of embryos scored for each genotype is given

in parentheses. **(C)** Absence of *Fgf8* expression and reduced domains of expression of *Six3* and *Hesx1* in the anterior brain parts of E8.5 *Lhx1<sup>+/−</sup>;Dkk1<sup>+/−</sup>* embryos (bottom panels), compared with the expression of the same markers in the wild type embryos (top panels). **(D)** RT-qPCR analysis of the expression of the WNT target *Axin2* (relative to *β-Actin*) in the anterior germ layer tissues of E7.75 early-bud to head-fold stage *Lhx1<sup>+/−</sup>;Dkk1<sup>+/−</sup>*, *Lhx1<sup>+/−</sup>*, *Dkk1<sup>+/−</sup>* and wild-type embryos. Data represent the mean ± standard errors of  $N = 5$  embryos analysed for each genotype, except  $N = 3$  for *Lhx1<sup>+/−</sup>* embryos.  $P$ -value < 0.01 (\*\*), no significant difference (ns) by t-test. **(E)** Truncated head phenotype of *Lhx1<sup>+/−</sup>;Dkk1<sup>+/−</sup>;Meox2<sup>+/−Cre</sup>* E9.5 mutant embryos. Lateral view of specimens with anterior side to the left, except for *en face* views. Scale bars: 100 μm.

**Table S1. Phenotypic analysis of *Lhx1*-epiCKO mutant embryos.**

Frequency of abnormal head phenotype for E8.5-E10.5 embryos generated from crosses between *Lhx1*<sup>fl/fl</sup> and *Lhx1*<sup>+/−</sup>; *Meox2*<sup>+/Cre</sup> mice.

Genotype	Number of embryos (number showing head abnormality)			
	<i>Lhx1</i> <sup>+/fl</sup>	<i>Lhx1</i> <sup>-/fl</sup>	<i>Lhx1</i> <sup>+/fl</sup> ; <i>Meox2</i> <sup>+/Cre</sup>	<i>Lhx1</i> <sup>-/fl</sup> ; <i>Meox2</i> <sup>+/Cre</sup>
	41 (0)	25 (0)	32 (1)	38 (38)
% with head defects	0%	0%	3.1%	100%

All the *Lhx1*<sup>-/fl</sup>; *Meox2*<sup>+/Cre</sup> mutant embryos displayed category V head defects.

**Table S2. Phenotypic analysis of *Lhx1*-ameCKO mutant embryos.**

**A.** Frequency of abnormal head phenotype for E9.5 embryos generated from crosses between *Lhx1*<sup>flox/flox</sup> and *Lhx1*<sup>+/−</sup>; *Foxa2*<sup>+/mcm</sup> or *Lhx1*<sup>+/−</sup>; *Foxa2*<sup>mcm/mcm</sup> mice injected with oil only (Mock) or tamoxifen (Tam).

Number of embryos (number showing head abnormality)								
Genotype	<i>Lhx1</i> <sup>+/flox</sup> ; <i>Foxa2</i> <sup>+/+</sup>		<i>Lhx1</i> <sup>+/flox</sup> ; <i>Foxa2</i> <sup>+/mcm</sup>		<i>Lhx1</i> <sup>flox/−</sup> ; <i>Foxa2</i> <sup>+/+</sup>		<i>Lhx1</i> <sup>flox/−</sup> ; <i>Foxa2</i> <sup>+/mcm</sup>	
Injection	Mock	Tam	Mock	Tam	Mock	Tam	Mock	Tam
	3 (0)	3 (0)	13 (4)	10 (2)	3 (0)	4 (1)	14 (2)	10 (9)
% with head defects	0%		31%		20%		0%	
	0%		31%		20%		0%	
	0%		31%		20%		0%	

**B.** Categories of the head phenotype of *Lhx1*<sup>flox/−</sup>; *Foxa2*<sup>+/mcm</sup> embryos.

	Number of embryos per head phenotype category					Number of embryo (%) with head defect
Phenotype category	I	II	III	IV	V	
Genotype						
<i>Lhx1</i> <sup>flox/−</sup> ; <i>Foxa2</i> <sup>+/mcm</sup> Mock	12	1	1	0	0	2 (14%)
<i>Lhx1</i> <sup>flox/−</sup> ; <i>Foxa2</i> <sup>+/mcm</sup> Tam	1	3	3	1	2	9 (90%)

P<0.01 by  $\chi^2$  test for the distribution of the embryos across the phenotype categories between the two treatment groups.

Affected embryos of the other genotypes (see part A) displayed category II phenotype.

**Table S3. Phenotypic analysis for genetic interaction of *Lhx1* and *Ctnnb1*.**

**A.** Frequency of abnormal head phenotype for E9.5 embryos generated from crosses between *Lhx1<sup>+/−</sup>* and *Ctnnb1<sup>Bfc/+</sup>* mice.

Genotype	Number of embryos (number showing head abnormality)			
	<i>Lhx1<sup>+/+</sup>;Ctnnb1<sup>+/+</sup></i>	<i>Lhx1<sup>+/−</sup>;Ctnnb1<sup>+/+</sup></i>	<i>Lhx1<sup>+/+</sup>;Ctnnb1<sup>Bfc/+</sup></i>	<i>Lhx1<sup>+/−</sup>;Ctnnb1<sup>Bfc/+</sup></i>
	20 (0)	21 (4)	17 (4)	17 (12)
% with head defects	0%	19%	24%	71%

**B.** Categories of head phenotype.

Phenotype category	Number of embryos per head phenotype category					Number of embryo (%) with head defect
	I	II	III	IV	V	
<i>Lhx1<sup>+/+</sup>;Ctnnb1<sup>+/+</sup></i>	20	0	0	0	0	0 (0%)
<i>Lhx1<sup>+/−</sup>;Ctnnb1<sup>+/+</sup></i>	17	2	2	0	0	4 (19%)*
<i>Lhx1<sup>+/+</sup>;Ctnnb1<sup>Bfc/+</sup></i>	13	3	1	0	0	4 (24%)+
<i>Lhx1<sup>+/−</sup>;Ctnnb1<sup>Bfc/+</sup></i>	5	1	10	1	0	12 (71%)*+

\*P<0.01 by  $\chi^2$ -test for difference in the distribution of the embryos across the phenotype categories between *Lhx1<sup>+/−</sup>;Ctnnb1<sup>Bfc/+</sup>* embryos and *Lhx1<sup>+/+</sup>;Ctnnb1<sup>+/+</sup>* embryos.

+P<0.01 by  $\chi^2$ -test for difference in the distribution of the embryos across the phenotype categories between *Lhx1<sup>+/−</sup>;Ctnnb1<sup>Bfc/+</sup>* embryos and *Lhx1<sup>+/+</sup>;Ctnnb1<sup>Bfc/+</sup>* embryos.

**Table S4. Phenotypic analysis for genetic interaction of *Lhx1* and *Dkk1*.**

**A.** Frequency of abnormal head phenotype for E8.5-E9.5 embryos generated from intercross of *Lhx1<sup>+/−</sup>;Dkk1<sup>+/−</sup>* mice.

Number of embryos (number showing head abnormality)				
Genotype	<i>Lhx1<sup>+/+</sup>;Dkk1<sup>+/+</sup></i>	<i>Lhx1<sup>+/−</sup>;Dkk1<sup>+/+</sup></i>	<i>Lhx1<sup>+/+</sup>;Dkk1<sup>+/−</sup></i>	<i>Lhx1<sup>+/−</sup>;Dkk1<sup>+/−</sup></i>
	6(0)	11 (1)	5 (0)	19 (14)
% with head defects	0%	9%	0%	74%

All *Lhx1<sup>+/−</sup>;Dkk1<sup>−/−</sup>*, *Lhx1<sup>−/−</sup>;Dkk1<sup>+/+</sup>*, *Lhx1<sup>+/−</sup>;Dkk1<sup>−/−</sup>*, *Lhx1<sup>−/−</sup>;Dkk1<sup>+/−</sup>* and *Lhx1<sup>−/−</sup>;Dkk1<sup>−/−</sup>* embryos also generated in this cross displayed defect as *Lhx1* or *Dkk1* homozygous null embryos (data not shown).

**B.** Categories of head phenotype.

	Number of embryos per head phenotype category					Number of embryo (%) with head defect
	I	II	III	IV	V	
Phenotype category						
<i>Lhx1<sup>+/+</sup>;Dkk1<sup>+/+</sup></i>	6	0	0	0	0	0 (0%)
<i>Lhx1<sup>+/−</sup>;Dkk1<sup>+/+</sup></i>	10	1	0	0	0	1 (9%)*
<i>Lhx1<sup>+/−</sup>;Dkk1<sup>+/−</sup></i>	5	0	0	0	0	0 (0%)†
<i>Lhx1<sup>+/−</sup>;Dkk1<sup>−/−</sup></i>	5	6	6	2	0	14 (74%)*†

\*P<0.01 by  $\chi^2$ -test for difference in the distribution of the embryos across the phenotype categories between *Lhx1<sup>+/−</sup>;Dkk1<sup>+/−</sup>* and *Lhx1<sup>+/−</sup>;Dkk1<sup>+/+</sup>* embryos.

†P<0.05 by  $\chi^2$ -test for difference in the distribution of the embryos across the phenotype categories between *Lhx1<sup>+/−</sup>;Dkk1<sup>+/−</sup>* and *Lhx1<sup>+/−</sup>;Dkk1<sup>−/−</sup>* embryos.

**Table S5. Phenotypic analysis for genetic interaction of *Lhx1* and *Dkk1* in the epiblast.**

**A.** Frequency of abnormal head phenotype for E8.5-E10.5 embryos generated from crosses between *Lhx1*<sup>flox/flox</sup> and *Dkk1*<sup>+/−</sup>; *Meox2*<sup>+/Cre</sup> mice.

Number of embryos (number showing head abnormality)				
Genotype	<i>Lhx1</i> <sup>+/flox</sup> ; <i>Dkk1</i> <sup>+/+</sup>	<i>Lhx1</i> <sup>+/flox</sup> ; <i>Dkk1</i> <sup>+/+</sup> ; <i>Meox2</i> <sup>+/Cre</sup>	<i>Lhx1</i> <sup>+/flox</sup> ; <i>Dkk1</i> <sup>+/−</sup>	<i>Lhx1</i> <sup>+/flox</sup> ; <i>Dkk1</i> <sup>+/−</sup> ; <i>Meox2</i> <sup>+/Cre</sup>
	34 (0)	33 (0)	32 (3)	25 (12)
% with head defects	0%	0%	9.5%	48%

**B.** Categories of head phenotype.

	Number of embryos per head phenotype category					Number of embryo (%) with head defect
Phenotype category	I	II	III	IV	V	
Genotype						
<i>Lhx1</i> <sup>+/flox</sup> ; <i>Dkk1</i> <sup>+/+</sup>	34	0	0	0	0	0 (0%)
<i>Lhx1</i> <sup>+/flox</sup> ; <i>Dkk1</i> <sup>+/+</sup> ; <i>Meox2</i> <sup>+/Cre</sup>	33	0	0	0	0	0 (0%)*
<i>Lhx1</i> <sup>+/flox</sup> ; <i>Dkk1</i> <sup>+/−</sup>	29	3	0	0	0	3 (9.5%)+
<i>Lhx1</i> <sup>+/flox</sup> ; <i>Dkk1</i> <sup>+/−</sup> ; <i>Meox2</i> <sup>+/Cre</sup>	13	8	3	1	0	12 (48%)*+

\*P<0.001 by  $\chi^2$ -test for difference in the distribution of the embryos across the phenotype categories between *Lhx1*<sup>+/flox</sup>; *Dkk1*<sup>+/−</sup>; *Meox2*<sup>+/Cre</sup> and *Lhx1*<sup>+/flox</sup>; *Dkk1*<sup>+/+</sup>; *Meox2*<sup>+/Cre</sup> embryos.

+P<0.01 by  $\chi^2$ -test for difference in the distribution of the embryos across the phenotype categories between *Lhx1*<sup>+/flox</sup>; *Dkk1*<sup>+/−</sup>; *Meox2*<sup>+/Cre</sup> and *Lhx1*<sup>+/flox</sup>; *Dkk1*<sup>+/−</sup> embryos.

**Table S6. Sequences of primers for RT-PCR and ChIP-PCR.****A. RT-PCR Primers.**

Gene	Sense primer	Antisense primer
<i>Pcdh1</i>	5'-GCTTCGTGTCAGTGTGCTT	5'-GTGTTTCGGTAGTCGCA
<i>Pcdh7</i>	5'-CCTGTACATAGAGGAGAACAA	5'-AGCTACTACTGTCCTGACAT
<i>Pcdh8</i>	5'-TTCAATGACAGTGACTCGGA	5'-GAAGGTTGACATCTGGGCT
<i>Pcdh9</i>	5'-CAGGAAAGCTGCAGTGACA	5'-ACATCTCTGTAGCTTCAGCT
<i>Pcdh9</i>	5'-TTCAGATCACTCAGTGCCT	5'-TCGAATGTGGAAACTGGTAG
<i>Pcdh10</i>	5'-CCAGGAAGCTGACATAGTAA	5'-AAGGGACAAAAGAAGGCATC
<i>Pcdh11x</i>	5'-ACTCGGCTATAAACTCTGA	5'-TTGAACAATCAGTTGGGCA
<i>Pcdh12</i>	5'-TCAATGGCAAAGTGTCTCCT	5'-TTATTTCCTCGGTGGTTGG
<i>Pcdh17</i>	5'-CAGTGACCAAGACACTAACAA	5'-ATCAGAACATGCCAAGCACTC
<i>Pcdh18</i>	5'-ATTCAGTGACCTCTTCCTCA	5'-TTGCTTCTGTAGTCAGAGGA
<i>Pcdh19</i>	5'-CACTATGATCTCGTGGCAA	5'-TGTCTTGCTCCTCACTATTG
<i>Pcdh20</i>	5'-CCAGTATGTGACCCTAAACA	5'-AACTCGGGAGCATTGTCATT
<i>Hesx1</i>	5'-AGCATTTAGGACTGGACCA	5'-ATGAAGTCTCACTGGGAAGA
<i>Cer1</i>	5'-GCATCGGTTCATGTTCAGAA	5'-GAACTCGATTTGCCAAAGCA
<i>Gsc</i>	5'-TGGAGAACCTTCCAGGA	5'-AGGATCGCTCTGTCGTCT
<i>Lef1</i>	5'-AACTGGCATCCCTCATCCA	5'-GCTACGACATTGCTCTCA

**B. ChIP-PCR primers.**

Region	Sense primer	Antisense primer
<i>Pcdh7</i> -0.2R	5'-TAGCAGTAAGGACTAACGCT	5'-TCCTGCTTCTCGAAAGTT
<i>Pcdh7</i> +8.5R	5'-GCACTAGTTAGTGGGAGAAA	5'-ACACTCAACCACAATGCTGA
<i>Dkk1</i> dH1	5'-CGAGGTTGATTGGATCA	5'-CACATGAGATCAAAGTGGCT
<i>Hesx1</i> dp	5'-CGTTCTGCTTAGGAGAGATA	5'-CCTTAGCTTGCTGACTA
<i>Gsc</i> U1	5'-TTAACGGCGGCAGGACAAT	5'-CCTTGGGTGGTGGAAAT
<i>Cer1</i> +4R	5'-TGATATCCCAGCTGGTCAAT	5'-AGAGCAAGCCAGAAGTTGA
Non target	5'-TGTTCCCGGAAGTGGTTAAT	5'-CTCTTATTGGTACTCCTGA

**SUPPLEMENTARY REFERENCES**

- Fossat, N., Le Greneur, C., Beby, F., Vincent, S., Godement, P., Chatelain, G. and Lamonerie, T.** (2007). A new GFP-tagged line reveals unexpected Otx2 protein localization in retinal photoreceptors. *BMC Dev Biol* **7**, 122.
- Fossat, N., Tourle, K., Radziewic, T., Barratt, K., Liebhold, D., Studdert, J. B., Power, M., Jones, V., Loebel, D. A. and Tam, P. P.** (2014). C to U RNA editing mediated by APOBEC1 requires RNA-binding protein RBM47. *EMBO Rep* **15**, 903-910.
- Tam, P. P. and Steiner, K. A.** (1999). Anterior patterning by synergistic activity of the early gastrula organizer and the anterior germ layer tissues of the mouse embryo. *Development* **126**, 5171-5179.